Atmospheric Environment 324 (2024) 120414

Contents lists available at ScienceDirect

Atmospheric Environment

journal homepage: www.elsevier.com/locate/atmosenv

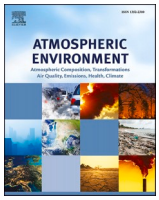

Characteristics of new particle formation events in a mountain semi-rural location in India

Jeni N. Victor [a], Pallavi Buchunde [a,b], Mathew Sebastian [c], Vijay P. Kanawade [c,d], Devendraa Siingh [a,*], Subrata Mukherjee [a], Swapnil S. Potdar [a], T. Dharmaraj [a], Govindan Pandithurai [a]

[a] Indian Institute of Tropical Meteorology, Ministry of Earth Sciences, Pune, India
[b] Savitribai Phule Pune University, Pune, India
[c] Centre for Earth, Ocean and Atmospheric Sciences, University of Hyderabad, India
[d] Climate and Atmosphere Research Centre, The Cyprus Institute, Nicosia, Cyprus

HIGHLIGHTS

- First direct observation-based estimates of sub-3 nm charged cluster formation and growth.
- New particle formation occurrence frequency was the highest in March through May months.
- Ions play an insignificant role in new particle formation in mountain semi-rural location.

ARTICLE INFO

Keywords:
Neutral and charged clusters
New particle formation
Growth rate
Mountain environment

ABSTRACT

Atmospheric new particle formation (NPF, via gas-to-particle conversion) occurs commonly in the troposphere which has implications for air quality, weather, and climate. Here, we comprehensively characterize NPF events at the High Altitude Cloud Physics Laboratory (HACPL) in a mountain semi-rural location, Mahabaleshwar using 2.5 years of semi-continuous measurements of ion and particle number size distributions. The occurrence frequency of NPF events was the maximum in March through May (pre-monsoon season) (22.9%) compared to other seasons. Considering all seasons at HACPL, the particle growth rates in the size range from 3 to 7 nm, 7–25 nm, and 5–25 nm varied from 0.5 to 6.9 nm h^{-1}, 1.3–10.2 nm h^{-1}, and 1.5–16.4 nm h^{-1}, respectively. The formation rate of charged clusters ($\mathbf{J_3^+}$ and $\mathbf{J_3^-}$) are reported for the first time from India, which ranges from 3.1 to 294.4 cm^{-3} s^{-1}. The general absence of a positive correlation between the particle formation rate and the growth rate indicates that dissimilar vapors might have contributed to the formation and growth of particles. Further, the role of ions in particle formation was also reported for the first time in India, which indicates an insignificant contribution of ions to particle formation at HACPL. At higher temperatures and lower relative humidity conditions, the formation rates of neutral/charged particles are found to be higher. Overall, our results provide new insights into NPF event characterization in the Indian context which have critical importance to an improved process-level understanding of secondary aerosol formation processes globally.

1. Introduction

Atmospheric new particle formation (NPF, via molecular clusters formation and their subsequent growth to larger sizes) occurs frequently in diverse environments, from remote polar to urban locations, around the world (Gautam et al., 2017; Kanawade et al., 2022a; Kerminen et al., 2018; Kulmala et al., 2004; Sellegri et al., 2019; Siingh et al., 2011; Wang et al., 2017; Nepolian et al., 2021). NPF events can take place over a spatial scale of hundreds of kilometers and a temporal scale of 1–2 days and are only observed when specific atmospheric conditions are met (Kulmala et al., 2014). Previous studies based on observations and modeling approaches suggest that NPF events produce about half of the present-day cloud condensation nuclei (CCN) (Gordon et al., 2017; Kerminen et al., 2012; Pierce and Adams, 2007; Sebastian et al., 2021a)

* Corresponding author.
E-mail address: devendraasiingh@tropmet.res.in (D. Siingh).

https://doi.org/10.1016/j.atmosenv.2024.120414
Received 13 February 2023; Received in revised form 3 February 2024; Accepted 18 February 2024
Available online 29 February 2024
1352-2310/© 2024 Elsevier Ltd. All rights reserved.

and thereby affecting cloud processes and radiative forcing (Sullivan et al., 2018). However, the fraction of newly formed particles that contribute to CCN formation remains poorly examined in diverse locations across the globe. A recent study showed that NPF-induced CCN production is higher in urban locations than in mountain-background locations in India (Sebastian et al., 2022).

NPF is a two-step process with the formation of small molecular clusters (sub-3 nm), then these clusters survive to grow to nucleation mode (particle diameter less than 25 nm) and Aitken mode particles (25–100 nm), eventually reaching CCN-active sizes (50–100 nm) under given atmospheric condition (Kulmala et al., 2012). Several investigators consistently reported and made significant improvements in the classification of NPF events and their characterization (Buenrostro Mazon et al., 2009; Dada et al., 2018; Dal Maso et al., 2005; Kamra et al., 2015; Kulmala et al., 2004, 2022a; Siingh et al., 2018). The combination of several factors is known to either favor or inhibit the NPF event in the atmosphere. Therefore, several aerosol nucleation predictors have been developed based on particle number size distribution measurements to examine NPF event occurrence in the atmosphere (Boy and Kulmala, 2002; Kerminen et al., 2018). As such the chemistry driving NPF event is still poorly examined globally, but the role of diverse chemical species involved in NPF events based on laboratory and ambient measurements has been investigated. For instance, sulfuric acid plays an important role in the initial part of the formation (clustering), and low-volatile organic compounds contribute most of the particle growth (Bianchi et al., 2016; Donahue et al., 2013; Ehn et al., 2014; Roldin et al., 2019; Smith et al., 2010; Zhao et al., 2020). The highly oxygenated molecules (HOMs) with extremely low volatility organic compounds (ELVOC), ammonia, amines, and ions (Bianchi et al., 2016; Kürten et al., 2016; Lehtipalo et al., 2018; Rose et al., 2018; Wagner et al., 2017) are also potential drivers of the NPF process. The recent novel 2019 Coronavirus (COVID-19) lockdown has provided us with a unique opportunity to detect, quantify and attribute the impacts of anthropogenic activities on the occurrence of NPF. While, the studies in Pune and Delhi (urban sites) found an increased occurrence of NPF under the reduced anthropogenic activities (Kamra et al., 2022; Yadav et al., 2021), Kanawade et al. (2022a) showed that NPF event occurrence was three-fold lower in Hyderabad (urban) during COVID-19 lockdown than in business-as-usual time periods. While the occurrence of NPF events was lower in Chennai during the COVID-19 lockdown, the rapid growth and high hygroscopicity of newly formed particles indicated high cloud-forming potential under the influence of sulfur plume (Singh et al., 2023). This suggests that the NPF phenomena are a non-linear dynamic process, with the timing of the NPF event in the atmosphere determined by the interplay of pre-existing particles, transported air masses, meteorological and dynamical conditions, and the source strength of condensable vapors.

In this study, we used atmospheric ions (in the diameter range of 0.36–47.1 nm) and particle number size distributions (5 nm–615 nm) from January 2015 to April 2017. Our main aim is to address the following known unknowns in the Indian context: 1) what is the frequency of occurrence of the regional NPF events at the mountain semi-rural site and its association with long-range transported air masses, 2) Do atmospheric ions play a role in the new particle formation event at our site? 3) What are the characteristics of NPF events such as the formation and growth rates of charged and neutral clusters?

2. Observation site and instrumentation

Ambient aerosol measurements were conducted at a High-Altitude Cloud Physics Laboratory (HACPL), Mahabaleshwar (17.92° N, 73.65° E, ~1378 m above mean sea level, hereafter referred to as HACPL). HACPL site experiences heavy rainfall (annual average rainfall ~5760 mm). The average annual temperature is 20 °C at the site. The station height remains above the mixed layer height (99–485 m above the ground) throughout the year (Aslam et al., 2021). Mahabaleshwar is situated at the hilltop of the Western Ghats Mountain ranges and is a tourist attraction town consisting of mixed deciduous forests, residential houses, hotels, and a rural market. Mahabaleshwar has a population of nearly 60,000 inhabitants and is located about 110 km to the south of Pune city. The site experiences local emissions from vehicular exhaust, biomass burning, and long-range transport from both continental polluted and marine air. The combination of complex sources which are active during the different times of the year (Buchunde et al., 2019; Mukherjee et al., 2018) and regional photochemistry make the site the best test-bed for studying aerosol aging and cloud formation processes (Mukherjee et al., 2020). Additionally, details of the site can be found in Mukherjee et al. (2018) and Leena et al. (2017). Here, the entire data is categorized into three seasons; pre-monsoon (March–May, MAM), post-monsoon (October–November, ON), and winter (December–February, DJF). There were no measurements during the Monsoon (June–September) due to persistently moderate to heavy rains and/or the site is mostly within the low shallow clouds during monsoon.

2.1. Neutral cluster and air ion spectrometer (NAIS)

NAIS measures ions of both polarities in the mobility range of 3.16–0.00133 $cm^2\ V^{-1}\ s^{-1}$ (diameter range 0.36–47.1 nm, 28 size bins), the method of diameter conversion from mobility has been adopted from Tammet (1995) and Horrak et al. (2000) (Table 1). Detailed information about the NAIS and the software can be found on the website: http://airel.ee and in Mirme and Mirme (2013). The uncertainty in the air ion concentration measurements is <10% (Wagner et al., 2016). Based on 200-s sample air and 100-s offset-level measurements, the average mobility of positive and negative ions is determined every 5 min. There are two basic categories, (i) charged clusters (mobility >0.5 $cm^2\ V^{-1}\ s^{-1}$; diameter <1.6 nm) and (ii) charged nanoparticles (mobility <0.5 $cm^2\ V^{-1}\ s^{-1}$; diameter >1.6 nm), that make up the total mobility distribution of atmospheric ions (Hõrrak et al., 2003). To estimate the formation rate of the neutral particles and sinks, particle concentrations in the size ranges of 3 nm–47.1 nm were also used. The instrument is deployed on the second floor at the height of 6 m in the three store buildings and the inlet is well exposed to the fresh wind circulation and guarded against the vertical electric field by the extended slab/floor. The complete details of the instrumentation can be found elsewhere (Mirme et al., 2007).

2.2. Wide range aerosol spectrometer (WRAS)

Particle number size distributions in the diameter range from 5 nm to 32 μm (72 size bins) were measured using a wide-range aerosol spectrometer (WRAS) with a time resolution of 5 min. Here, we used particle number size distribution measurements in the size range from 5 nm to 1000 nm (53 size bins). WRAS, manufactured by GRIMM, Germany. The WRAS system consists of a scanning mobility particle sizer (SMPS) with a condensation particle counter (SMPS + C; CPC model 5.4) and a light scattering optical particle size spectrometer (Opt. Spect.; GRIMM EDM 180). The SMPS + C consisting of a differential mobility analyzer (DMA) measures the particle size distribution in the electrical mobility size

Table 1
Classification of different events considered in this study.

NPF	An abrupt increase in sub-3 nm ions and nucleation mode particles (sub-25 nm) with evidence of steady growth in the ion and particle size, thus appearing as conventional banana-shaped ion and aerosol growth. Ion and particle mode diameter is lesser than 3 nm and 25 nm, respectively, so that the growth rate and formation rate of ions and particles can be calculated.
Non-event	No increase in sub-3nm ions and nucleation mode particles (sub-25nm) and ion and particle mode diameter (absence of growth) during the day
Undefined	All the remaining valid observation days which doesn't satisfy either of the above two criteria,

range of 5–350 nm in 45 channels by stepwise changing the DMA voltage. An optical spectrometer works on the basic principle of the light-scattering of a single particle. A PIN-diode is used to detect the scattered light, and the signals are then amplified and divided into 31 size channels in the 250 nm to 32 μm optical diameter range, they are automatically synchronized by the software. This device is well-protected for room-temperature operation under the air conditioning system. We used a Nafion dryer to lower the relative humidity of the air sample to 40%.

2.3. Meteorological parameters and air mass history

Meteorological parameters such as temperature and relative humidity (RH) were obtained using an automatic weather station (AWS) at a temporal resolution of 1 min. The measurement site experiences north-westerly winds in pre-monsoon, and south-easterly winds in the post-monsoon and winter seasons (Mukherjee et al., 2020). We have also performed airmass backward trajectory calculations using the National Oceanic and Atmospheric Administration (NOAA) Hybrid Single Particle Lagrangian Integrated Trajectory (HYSPLIT) model (Draxler and Rolph, 2014), to examine the influence of airmass history on new particle formations.

3. Analysis methods

3.1. Classification of the events

An NPF event is generally identified by the visual inspection of the shape characteristic of particle number size distributions and characteristic properties such as formation rate and growth rate of particles (Dal Maso et al., 2005; Hirsikko et al., 2007). Here, we classified events into three different types: NPF, non-events, and undefined (Table 1). The time evolution of particle number size distribution shows the temporal change in concentrations throughout the observation time period from January 2, 2015 to April 30, 2017 (Fig. S1).

3.2. Ion and particle formation and growth rates

The particle growth rates (GR) of the newly formed ions or particles can be determined from the measured ion or particle number size distributions (Hirsikko et al., 2007; Kulmala et al., 2012). GRs were obtained by a linear least-square fit through the temporal variation of particle mode diameter of the measured particle number size distributions. The particle diameter corresponding to the maximum number concentration of particles is referred to as the particle mode diameter (Figs. S5 and S6) through which a first-order polynomial fitted to calculate particle growth rate. GRs were calculated for the particle size ranges 3–7 nm, 7–25 nm from NAIS and 5–25 nm from WRAS measurements.

The formation rate of 3 nm particles was calculated using the following equation:

$$J_3 = \frac{dN_{3-7}}{dt} + CoagS_{3-7} \,.\, N_{3-7} + \frac{1}{1nm} GR_{3-7} N_{3-7} \quad (1)$$

where N_{3-7} is the negative particle concentration between 3 and 7 nm from NAIS, $CoagS_{3-7}$ is the coagulation sink of 3–7 nm particles and GR_{3-7} is the particle growth rate in the size range of 3–7 nm (Kulmala et al., 2007).

The formation rate of charged particles (both positive and negative) of 3 nm were calculated using the following equation,

$$J_3^{\pm} = \frac{dN_{3-7}^{\pm}}{dt} + CoagS_{3-7} \,.\, N_{3-7}^{\pm} + \frac{1}{1nm} GR_{3-7} N_{3-7}^{\pm} + \alpha \,.N_{3-7}^{\pm}\, N_{<7}^{\mp} - \beta \,.N_{3-7}\, N_{<7}^{\pm} \quad (2)$$

where $N_{3-7}^{\pm}$ refers to the 3–7 nm charged particle concentration, $N_{<7}^{\mp}$ the sub-7 nm charged particle concentration of the opposite polarity. Here, the ion-ion recombination coefficient was taken as 1.6×10^{-6} cm^3 s^{-1} (Israel, 1971), and the ion-neutral attachment coefficient was taken as 0.01×10^{-6} cm^3 s^{-1} (Hoppel, 1985).

The formation rate of particles of size 5 nm was calculated using the following equation:

$$J_5 = \frac{dN_{5-25}}{dt} + CoagS_5 \,.\, N_{5-25} + \frac{1}{20nm} GR_{5-25} N_{5-25} \quad (3)$$

where N_{5-25} is the particle concentration between 5 and 25 nm, $CoagS_5$ is the coagulation sink of 5 nm particles and $GR_{5\text{-}25}$ is the particle growth rate in the size range of 5–25 nm.

3.3. Contribution of ions to particle formation

The total nucleation rate (J) can be expressed as the sum of neutral and ion-induced nucleation rates (Manninen et al., 2009). Following the Manninen et al. (2010) methodology, the ion-ion recombination was omitted from the neutral particle formation rate. Therefore, it is the ion-induced fraction and not the ion-mediated nucleation fraction. The contribution of ions to particle formation is thus calculated as given below;

$$IIN = \left(J_3^{+} + J_3^{-}\right)/J_3 \quad (4)$$

4. Results and discussion

4.1. Frequency of occurrence of NPF events

Fig. 1 shows the percentage occurrence of the event days per season at HACPL in Mahabaleshwar. Overall, out of 540 valid observation days, NPF events occurred on 79 days (14.6%) and non-events were observed on 353 days (65.4%) at HACPL (monthly frequency of NPF event classifications is given in Fig. S3). A total of 108 undefined days (20%) were categorized as the days that could not be classified as NPF event or non-events days due to mixed features such as broken banana-shaped aerosol growth, ion/particle bursts without evidence for growth (volcano/apple), or Aitken mode growth or tail events (Buenrostro Mazon et al., 2009; Kanawade et al., 2014b). A recent study in India showed that more than half of events days with particle bursts (volcano/apple) in the sub-3nm size range did not show banana-shaped aerosol size growth during summer (March through May) (Sebastian et al., 2021b). The frequency of occurrence of NPF events was the highest in MAM months

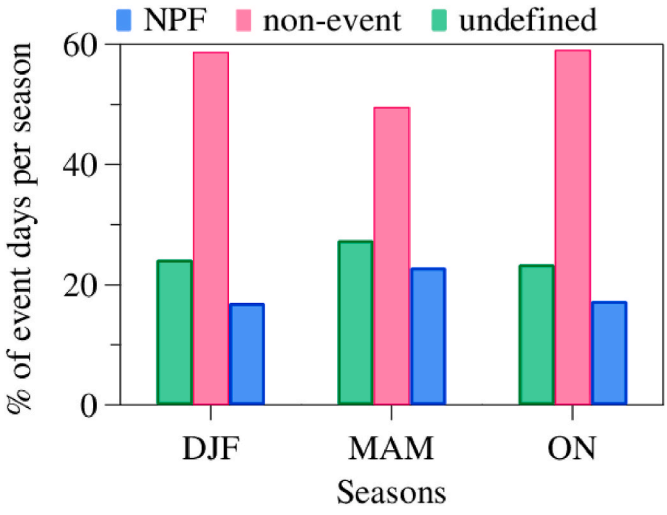

Fig. 1. The percentage of occurrence of different types of events during each season. DJF→ December, January, February; MAM→ March, April, May; ON→ October, November.

(22.9%), mainly due to the high solar radiation (typically higher oxidation extent of the atmosphere enhancing the production of low volatile organic compounds responsible for particle growth) and relatively low pollution loading close to the surface (owing to dilution effect from elevated boundary layer resulting lower condensation sink for condensable vapors, Fig. 3e). While, in the Indian context, the frequency of occurrence of NPF events is the lowest during the monsoon due to efficient wet scavenging of aerosol precursor gas concentration and weak gas-phase oxidation chemistry under diminished solar radiation on persistently cloud days (Kanawade et al., 2014b, 2022a), the lowest frequency of occurrence of NPF events was observed in winter (16.9%). Overall, the seasonal variation in the occurrence of NPF events is similar to other sites in India and globally (Kerminen et al., 2018; Kulmala et al., 2004; Sebastian et al., 2022; Wang et al., 2013). It should be noted that there are a few exceptions when researchers observed the highest NPF event frequency in winter (Xiao et al., 2015; Zhu et al., 2017).

Fig. 2 shows the average of all the observed NPF events, non-events, and undefined events based on measured particle number size distributions from WRAS and NAIS. On NPF event days (Fig. 2a), the particle bursts followed by sustained growth in particle size are evident during the day. After sunrise, the atmospheric dilution effect reduces the condensation sink sufficiently for the NPF event to trigger. The increase in neutral cluster and nucleation mode particles is evident and the NPF event continued beyond midnight till the next day morning at 10:00 a.m. local time (not shown in the Figure). Such regional NPF events occur over a spatial scale of 100's kilometers and a temporal scale of 1–2 days (Kerminen et al., 2018; Kulmala et al., 2012, 2013). On non-event days, no significant changes are evident in particle number size distributions and particle mode diameter during the course of the day, indicative of non-event days (Fig. 2b). Lastly, the day which was not able to classify either NPF event or non-event was referred to as an undefined event day (Fig. 2c). The particle number size distributions showed irregularities and the Aitken mode growth was evident in the late afternoon and evening hours. The exact reason for such irregularities is not known but it could be due to the mixing of different air masses (inhomogeneity) or sudden changes in environmental conditions (temperature, relative humidity, wind, precursor gas, or background aerosol concentration).

4.2. *Characteristics of event types*

To illustrate the characteristics of different event types, the size-segregated particle number concentrations, condensation sink, and coagulation sink were derived from WRAS particle number size distribution data (Fig. 3). Nucleation mode particles ($N_{5–25nm}$) are mainly

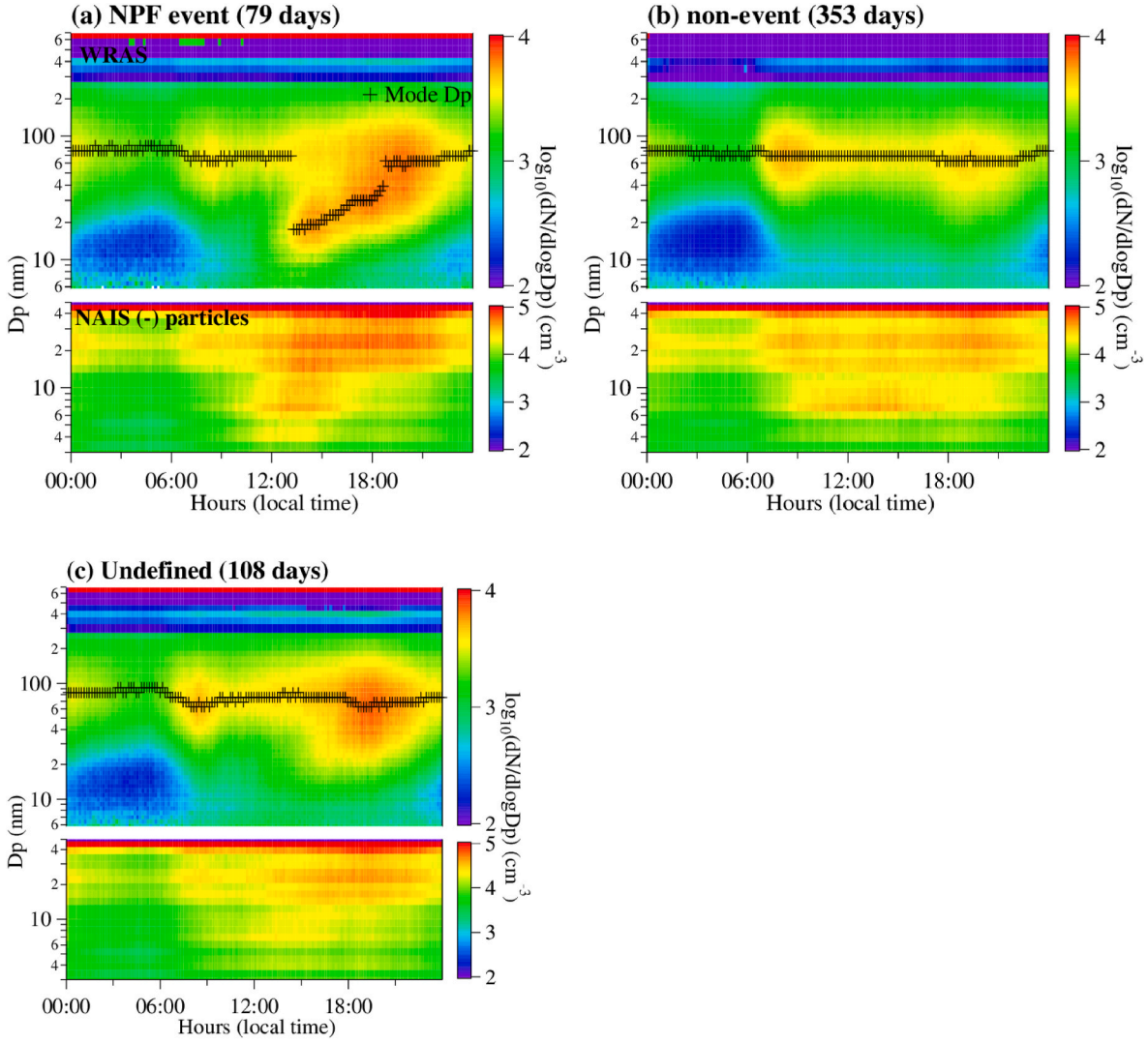

Fig. 2. Time evolution of averaged particle number size distributions in the size range from 5 to 680 nm from WRAS (top panel) and negative particle number size distribution in the size range 1–47 nm from NAIS (bottom panel) for observed (a) NPF events (79 days) (b) non-events (353 days), and (c) undefined events (108 days). The solid black line indicates the particle mode diameter.

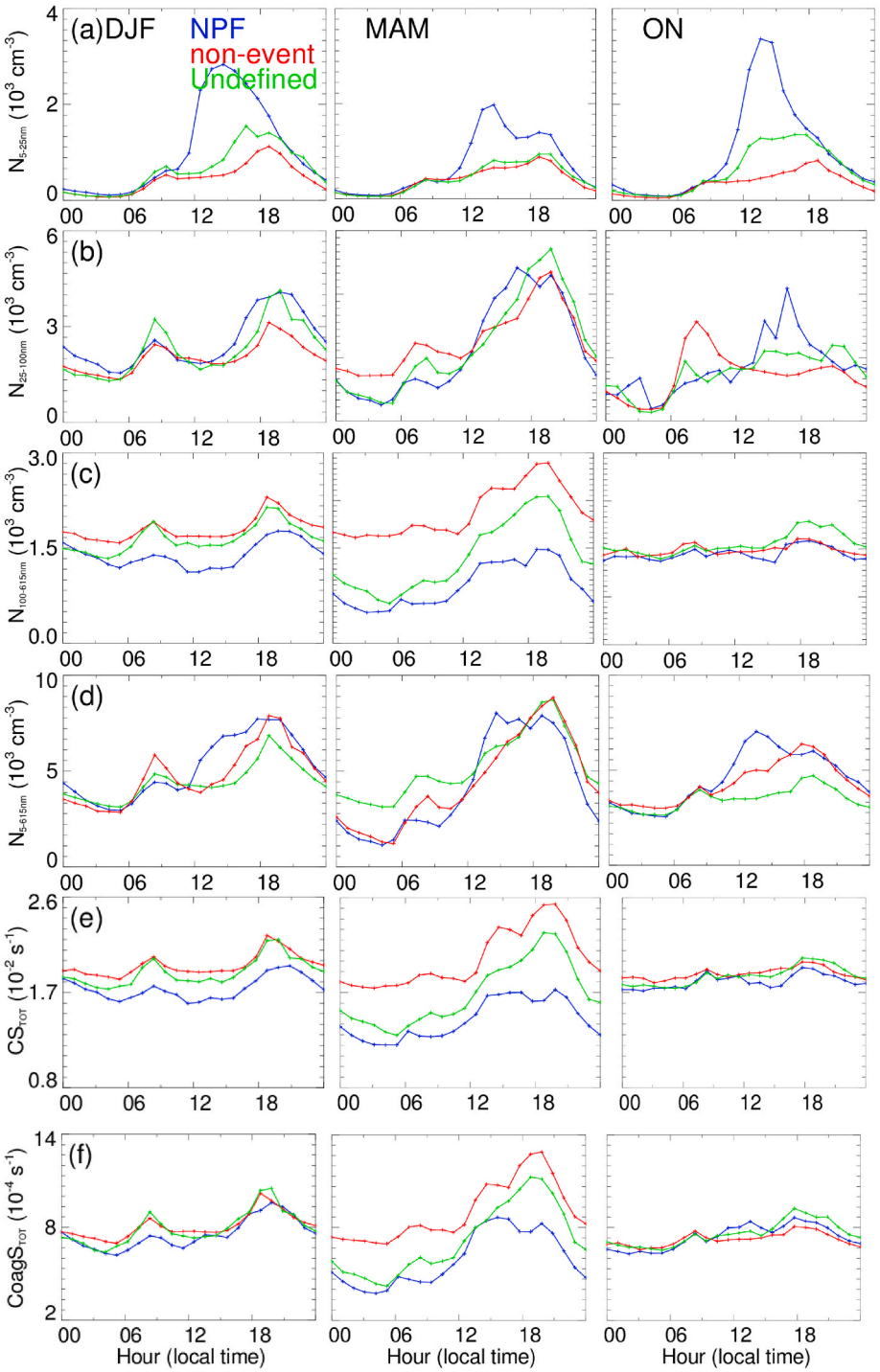

Fig. 3. Median diurnal variation of (a–d) size-segregated particle number concentrations, (e) total coagulation sink (CS_{TOT}), and (f) total coagulation sink ($CoagS_{TOT}$) for observed NPF events (blue), non-events (red), and undefined events (green).

derived from the atmospheric NPF, while Aitken mode particles ($N_{25–100nm}$) are derived from either direct primary anthropogenic emissions or secondary aerosol formation and growth processes or both. The accumulation mode particles ($N_{100–615nm}$) are mainly derived from direct primary anthropogenic emissions or growth of Aitken mode particles (both primary and secondary). The condensation sink (CS_{TOT}) indicates the vapor loss due to condensation on to pre-existing particles while the coagulation sink ($CoagS_{TOT}$) indicates particle loss by particle-particle coagulation. Fig. 3 shows the averaged diurnal variation of size-segregated particle number concentrations, total condensation sink, and total coagulation sink on the observed NPF event, non-event, and undefined event days during different seasons. The $N_{5–25nm}$ on NPF event days were significantly higher than non-event and undefined days in all seasons considered in this study (Fig. 3a) indicating that NPF is a significant source of aerosol numbers to the atmosphere. While $N_{25–100nm}$ did not show any differences between event types, $N_{100–615nm}$ were the lowest during NPF events indicating that NPF does not contribute significantly to accumulation mode particles and therefore to the total aerosol mass. The CS_{TOT} on NPF event days was lower than that of non-event and undefined days indicating that NPF is favored at lower pre-existing particle concentration. Most studies showed that NPF is often associated with lower condensation sink (Dal Maso et al., 2005;

Zhang et al., 2010, Kulmala et al., 2004, Kerminen et al., 2018), while urban locations in developing countries report the highest formation and growth rates at higher condensation sink (Kanawade et al., 2022b; Kulmala et al., 2021; Yu et al., 2016). The CoagS_{TOT} on NPF was also lower than that of non-event and undefined days. Considering all seasons, $N_{5–25nm}$ ranged from 1.2 to 3.7 × 10^3 cm^{-3}, with a mean and standard deviation of (1.1 ± 1.5) × 10^3 cm^{-3}. $N_{5–615nm}$ ranged from 0.1 × 10^3 to 103.3 × 10^3 cm^{-3}, with a mean and standard deviation of (5.2 ± 5.1) × 10^3 cm^{-3}.

4.3. Formation and growth rates of ions and particles

The strength of an NPF event is quantified by calculating the formation rate and growth rate of particles for a size range of interest. Fig. 4 shows size-segregated (3–7 nm, 7–25 nm, and 5–25 nm) growth rates of particles for different seasons. The growth rates for the first two size ranges (i.e., 3–7 nm, and 7–25 nm) were obtained from NAIS negative particle data while the growth rate in the size range from 5 to 25 nm was obtained from WRAS particle data. The median growth rates of particles in the size range of 3–7 nm, 7–25 nm, and 5–25 nm when averaged over all seasons were 2.9, 4.6, and 4.5 nm h^{-1}, respectively. The size-segregated growth rates of particles in all size ranges were the highest during MAM as compared with DJF and ON. The size-dependency of the particle growth rates is also consistent with earlier observations from SMEAR II station Hyytiälä, Finland (Manninen et al., 2009), Tumbarumba in Australia (Suni et al., 2008), K-puszta (Yli-Juuti et al., 2009) and Granada, Spain (Casquero-Vera et al., 2020). The increasing growth rate with increasing size range suggests the variable degree of contribution of chemical vapors to the growth (Guo et al., 2014). The growth rates observed at HACPL are significantly lower than those observed in heavily polluted environments such as Mexico City (15–40 nm h^{-1}; Iida et al. (2008) or South Africa (3–21 nm h^{-1}; Laakso et al. (2008) and Beijing (7.8 nm h^{-1}; Zhou et al. (2021)) to moderate or semi-urban environments (mountain or high-altitude stations) such as Beijing (6.5 nm h^{-1}; Zhou et al., 2021). The pattern of decreasing growth rate from urban to rural indicates the reduced strength of precursors loading required for particle growth in the rural environment (Wang et al., 2013). Similar to the observed variation in the frequency of occurrence of NPF events at HACPL, the particle growth rates were slightly higher in MAM months (summer/pre-monsoon) than in other months. The seasonal cycle in particle growth rates is consistent with that observed previously in Mahabaleshwar (Sebastian et al., 2022) and elsewhere (e.g. Baalbaki et al., 2021; Chu et al., 2019). The size-segregated growth rate of particles is well within the wide range of values seen in diverse environments around the world (e.g., Kanawade et al., 2022b; Kerminen et al., 2018; Kulmala et al., 2004; Manninen et al., 2010; Wang et al., 2013).

Fig. 5 shows the median diurnal variation of particle formation rate of 3 nm (charged and neutral) and 5 nm particles. The charged and neutral particle formation rates start increasing in the early morning (04:00–06:00 LT) peaking at noontime (11:00–13:00 LT), and then gradually decreasing as the day passed. While the steady increasing pattern of charged and neutral particle formation rates indicates the survival of newly formed cluster ions or particles against their coagulational loss to pre-existing particles, the steady decreasing pattern of charged and neutral particle formation rates indicates that the condensational growth outweighs the formation rate later during the day. The magnitude and the seasonal pattern of the formation rate of 5 nm particles were comparable with that previously observed in Mahabaleshwar (Sebastian et al., 2022) and elsewhere globally (Chu et al., 2019; Kerminen et al., 2018). In Beijing, J showed a clear seasonal variation with maxima in winter and minima in summer, while the observed GR did not show a clear seasonal pattern (Deng et al., 2020). The ambient temperature was found to be a governing factor for driving seasonal patterns in J in Beijing. In Mahabaleshwar, J did not show a clear seasonal pattern while FR showed a distinct seasonal pattern with maxima in summer and minima in winter. It seems to us that the relatively higher ambient temperature (20–25 °C) in Mahabaleshwar when compared to Beijing might be a governing factor for driving seasonal patterns in GR in Mahabaleshwar, providing more low-volatility oxygenated vapors for condensational growth. Compared to other high-altitude sites globally (Cai et al., 2021; Lv et al., 2018; Shang et al., 2018; Tröstl et al., 2016; Yue et al., 2013), the formation rate of 3 nm neutral particles (J_3) is higher by two orders of magnitude at Mahabaleshwar (47 - 1901 cm^{-3} s^{-1}). Further, the formation rate at 3 nm neutral particles varied within the same order of magnitude between different seasons, peaking during ON season.

Table 2 summarizes the seasonal median size-segregated growth rates, the formation rate of 3 nm charged clusters of both polarities and neutral, the formation rate of 5 nm particles, and the contribution of ion-induced nucleation to the total particle formation rate of 3 nm particles for the observed NPF events at HACPL in Mahabaleshwar. The median size-segregated growth rates are the highest in the pre-monsoon while the median formation rates of ions and particles are the maximum in the winter season. The $GR_{5–25nm}$ (7.9 ± 3.5 nm h^{-1}) in MAM at HACPL was also comparable to that in urban locations such as Pune (7.8 ± 1.7 nm h^{-1}) (Siingh et al., 2013) and Kanpur (8.7 ± 3.2 nm h^{-1}) (Kanawade et al., 2014b). Considering all seasons at HACPL, Mahabaleshwar, $GR_{3–7nm}$, $GR_{7–25nm}$, and $GR_{5–25nm}$ varied from 0.5 to 6.9 nm h^{-1}, 1.3–10.2 nm h^{-1}, and 1.5–16.4 nm h^{-1} respectively. Throughout all seasons, the formation rate of 3 nm particles ranged from 47 to 1901 cm^{-3} s^{-1}, the formation rate of 3 nm positive (negative) ions ranged from 3.1 to 81 cm^{-3} s^{-1} (3.6–294 cm^{-3} s^{-1}), and the formation rate of 5 nm particles ranged from 0.45 to 3.5 cm^{-3} s^{-1}. Further, the calculated IIN fraction ranged from 0.07 to 0.39, suggesting that the contribution of ions to particle formation was insignificant at our site, analogous to that observed at other sites (Kulmala et al., 2007). Table 2 also summarizes seasonally averaged NPF event characteristics from the low altitude semi-rural and high-altitude mountain locations across the globe. Overall NPF event characteristics at HACPL are comparable to similar locations across the globe.

Fig. 6 shows the scatter plot of the growth rate of 3–7 nm particles

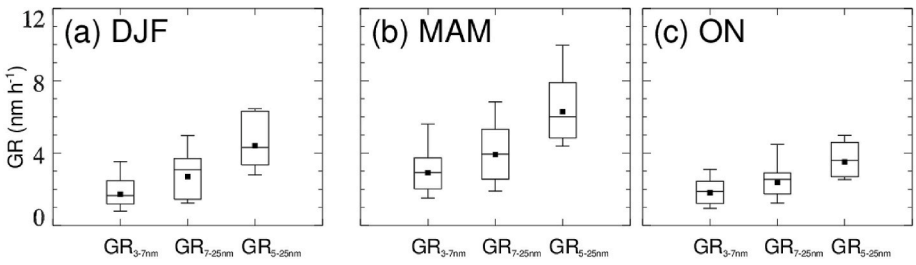

Fig. 4. Box–whisker plot of size-segregated growth rates of particles (3–7 nm, 7–25 nm, and 5–25 nm) for (a) DJF, (b) MAM), and (c) ON. The solid square indicates the mean, the horizontal line indicates the median, the top and bottom of the box indicate the 25th and 75th percentile values and the top and bottom whiskers indicate the 10th and 90th percentile values. DJF→ December, January, February; MAM→ March, April, May; ON→ October, November. Note that $GR_{3–7nm}$ and $GR_{7–25nm}$ were derived from NAIS negative particle data while $GR_{5–25nm}$ was derived from WRAS particle data.

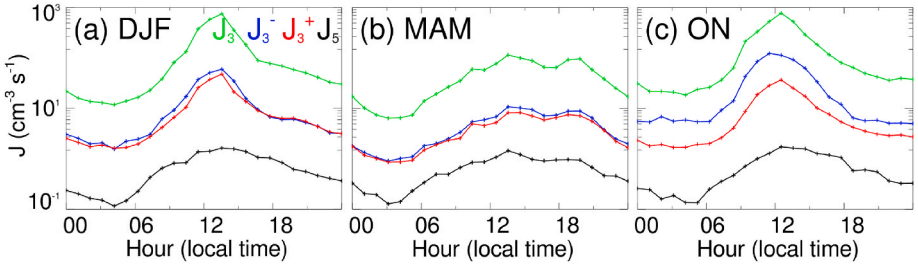

Fig. 5. Diurnal variation in median J_3, J_3^-, J_3^+ and J_5 for (a) DJF, (b) MAM, and (c) ON months. DJF→ December, January, February; MAM→ March, April, May; ON→ October, November.

Table 2
Summary of median (8:00 a.m. to 4:00 p.m. local time) $GR_{3–7nm}$, $GR_{7–25nm}$, $GR_{5–25nm}$, J_3, J_3^-, J_3^+, J_5 and the observed fraction of ion-induced nucleation (IIN) on the observed NPF events at HAPCL site and other selected similar locations across the globe. "±" indicates the standard deviation. "-" indicates no data.

Location	Site type	Season		$GR_{3–7nm}$	$GR_{7–25nm}$	$GR_{5–25nm}$	J_3	J_3^-	J_3^+	J_5	IIN (fraction)	Reference
				(nm h^{-1})			(cm^{-3} s^{-1})					
Mahabaleshwar, India	Mountain semi-rural	DJF	Range	0.5–5.0	2.6–6.5	2.1–10.1	70–1901	7.7–80	4.9–81	0.44–3.5	0.08–0.23	This study
			Mean	2.7 ± 1.3	4.4 ± 1.3	4.7 ± 2.2	419 ± 459	28 ± 22	19 ± 19	1.0 ± 0.63	0.10 ± 0.04	
			Median	2.8	4.3	4.1	272	20	13	0.77	0.13	
		MAM	Range	1.3–6.9	2.9–10.2	3.4–16.4	47–449	3.6–102	3.1–18	0.45–1.70	0.07–0.39	
			Mean	3.9 ± 1.6	6.3 ± 2.0	7.9 ± 3.5	130 ± 89	14 ± 20	6.8 ± 3.7	0.80 ± 025	0.20 ± 0.07	
			Median	3.9	6	7.5	107	6.2	6.1	0.77	0.14	
		ON	Range	1.2–4.5	1.3–5.0	1.5–9.8	143–1259	22–294	5.6–60	0.45–2.1	0.13–0.38	
			Mean	2.4 ± 0.9	3.5 ± 1.0	3.7 ± 2.5	478 ± 325	88 ± 77	18 ± 15	1.0 ± 0.47	0.20 ± 0.06	
			Median	2.5	3.6	2.5	378	67	10	0.97	0.19	
Mahabaleshwar, India	Mountain semi-rural	Annual	Mean	–	–	4.7 ± 3.0	–	–	–	0.04 ± 0.02	–	Sebastian et al. (2022)
Mt. Yulong, China	Mountain background	MA	Mean	3.22[a]	–	–	1.18	–	–	–	–	Shang et al. (2018)
Mt. Tai, China	Mountain	JASON	Mean	1.98[b]	–	–	7.10	–	–	–	–	Lv et al. (2018)
Jungfraujoch, Switzerland	Mountain background	Annual	Mean	–	–	4.0[c]	1.8[d]	–	–	–	–	Tröstl et al. (2016)
Pearl River Delta, China	Rural site	July	Range	–	–	4.0–22.7	2.4–4.0	–	–	–	–	Yue et al. (2013)
Wudang, China	Mountain background	June	Range	–	–	0.3–11.4[e]	0.6–6.9	–	–	–	–	Cai et al. (2021)

[a] $GR_{3–25nm}$.
[b] $GR_{3–20nm}$.
[c] $GR_{5–15nm}$.
[d] $J_{3.2}$.
[e] GR_{3-30}.

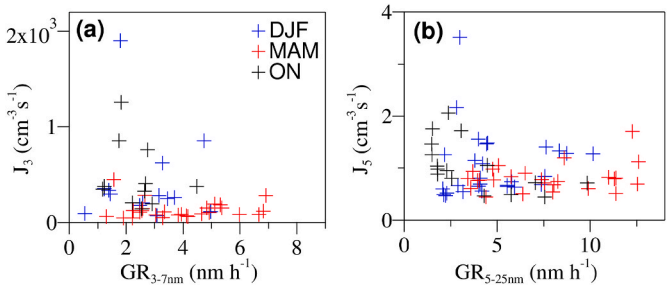

Fig. 6. Scatter plot between particle growth rates and formation rates for each season, (a) $GR_{3–7nm}$ and J_3 and (b) $GR_{5–25nm}$ and J_5. DJF→ December, January, February; MAM→ March, April, May; ON→ October, November.

versus the particle formation rate of 3 nm particles and the growth rate of 5–25 nm particles versus the particle formation rate of 5 nm particles. The general absence of a good positive correlation between the particle growth rates and the particle formation rates for both size ranges (3–7 nm and 5–25 nm) indicates the role of the different vapor sources involved in particle formation and growth (Birmili et al., 2003). This corroborates the finding above showing different seasonal patterns in particle growth rate and the formation rate. Sulfuric acid cluster formation in the atmosphere follows its stabilization by the presence of bases like amines/ammonia (Kuang et al., 2008; Paasonen et al., 2010) or highly oxygenated molecules (Schobesberger et al., 2013), a recent study showed that oxidation of aromatic compounds forming highly oxygenated molecules plays a minimal role in particle formation (Xiao et al., 2021). A recent study in India showed that sulfuric acid plays an important role in the sub-3 nm neutral cluster formation, and hypothesized that volatile organic compounds might have contributed significantly in the particle growth as sulfuric acid could explain only 5–25% of the observed total particle growth (Sebastian et al., 2021b). Kulmala et al. (2022b) further demonstrated that highly oxygenated molecules and sulfuric acid together could not explain the observed growth and therefore the more complex multi-phase chemistry is involved in particle formation and growth, particularly in polluted environments.

Indeed, the formation of secondary aerosols is a strong function of temperature, humidity, wind speed as well as gas-phase chemicals and particles in the atmosphere, in light of this, the chemistry underlying NPF event is dynamically complex and varies depending on the type of place (Guo et al., 2014; Kulmala, 2015). As such, in the Indian context, very little is known about the physio-chemical processes driving new particle formation in diverse environments (Kanawade et al., 2022b).

4.4. Influence of meteorological parameters and air mass history on NPF

NPF is strongly influenced by given atmospheric conditions such as temperature (or solar radiation), relative humidity, and wind speed (Hakala et al., 2022; Kerminen et al., 2018; Kulmala et al., 2004). A recent study showed that the formation of sulfuric acid-base clusters favors at low temperatures (Xiao et al., 2021) while most previous studies showed that NPF rates are higher at higher temperatures or solar radiation (Kanawade et al., 2014a; Kulmala et al., 2004; Shen et al., 2011; Siingh et al., 2018; Stanier et al., 2004). Generally, we observed the largest NPF rates at higher temperatures and lower relative humidity analogous to previous studies (Fig. 7). At higher altitude stations, the mean temperature is usually lower than at low altitudes, which leads to less evaporation and more condensational growth of the particles. NPF is usually not favored at high relative humidity conditions due to the hygroscopic growth of pre-existing particles and/or weak gas-phase oxidation rates under cloudy conditions. Kulmala et al. (2002) reported that higher (lower) relative humidity intrigues the negative (positive) feedback on the solar radiation intensity and hence gas-phase photochemical chemistry, which can hinder (promote) the formation of particles. Rose et al. (2015) confirmed from the measurement at Chacaltaya, Bolivia (5.2 km amsl) finding higher NPF frequency occurred during the dry season (less RH). However, some of the exceptions (no significant relation with RH) were also reported at Maido station (2.1 km amsl) and high-altitude station, Beijing (2.5 km amsl), (Casquero-Vera et al., 2020; Foucart et al., 2018). In addition, high RH was also found to be associated with more clouds, resulting in less solar radiation (Dada et al., 2018) and hence photochemical activity (Zhou et al., 2021). The increased surface temperature enhances gas-phase oxidation and air dilution increasing boundary layer mixing height which results in lower condensation sink near the surface, thus providing favorable conditions for the particle formation (Kulmala et al., 2002). The temperature, along with other parameters and their feedback, determines whether particle formation will occur, but it also determines if the NPF event will proceed in the atmosphere. The strong and obvious negative correlation between temperature and relative humidity with high NPF rates at high

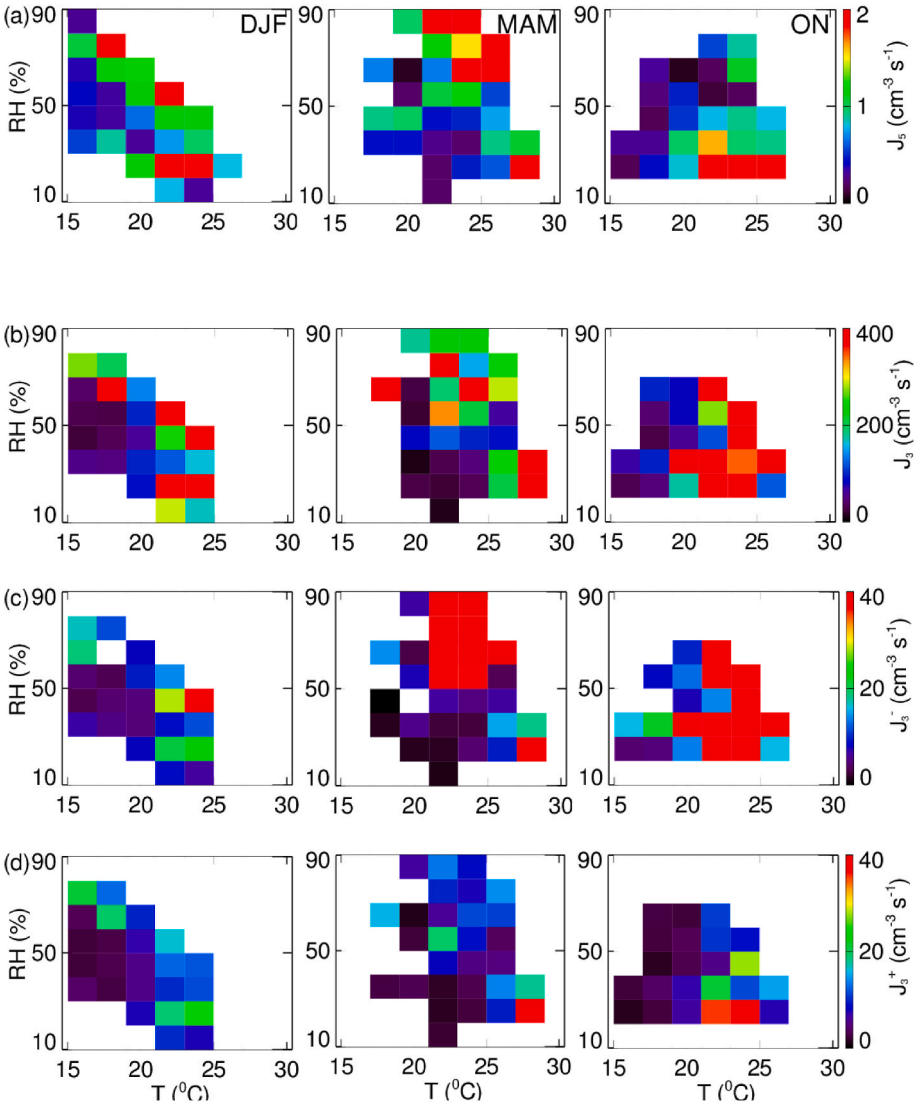

Fig. 7. Contour plot of temperature versus relative humidity as a function of the particle formation rate (a) J_5, (b) J_3, (c) J_3^-, and (d) J_3^+) for DJF (left column), MAM (middle column), and ON months. DJF→ December, January, February; MAM→ March, April, May; ON→ October, November.

temperatures and lower relative humidity is observed at HACPL. While high concentrations of volatile organic compounds are thought to enhance NPF rates at high temperatures, the co-emission of NO_X can suppress nucleation, particularly in polluted environments (Xiao et al., 2021). This suggests that the interplay between gas-phase chemistry and atmospheric conditions may be entirely different for NPF processes between clean and polluted environments.

Further, several investigators showed that NPF event is also strongly driven by the air mass history and its modification (Asmi et al., 2011; Hamed et al., 2007; Kanawade et al., 2012; Nieminen et al., 2014). Fig. 8 shows a 3-day air mass backward trajectory starting at 500 m above the ground level at 6 UTC (11:30 a.m. local time) at the HACPL site calculated from the HYSPLIT model. The HACPL site experiences air masses from north-east and east during ON and DJF months while from south-west and west during MAM months. Interestingly, air mass origin between NPF and non-event days appears to be the same mostly, except for about 15% of days when air mass origin was different on non-events days than on NPF event days. This suggests that the source region of the air mass is not the critical factor for the occurrence of the NPF event at this site. It seems to us that the modification of the air mass as it travels in the atmosphere decides whether an NPF event will trigger or inhibit within the given air mass. Tunved et al. (2006) showed that pristine air entering a boreal forest zone triggers NPF event as air mass traveled over the forest (possibly triggered by biogenic volatile organic compounds such as monoterpenes in the presence of ozone or other oxidants) and then maintained over the forested area until the high pre-existing aerosols finally terminate it. Later Foucart et al. (2018) reported that the amount of clean/polluted air present in the transported airmass decides the intensity of NPF event rather than its frequency. In addition to supporting the development of NPF events by clean air mass associated with low-condensation sinks at high-altitude sites, vertical motions of air masses from lower altitudes also affect particle formation (Zhou et al., 2021). Another recent study by Petäjä et al. (2022) showed that the intrusion of marine air masses into the SMEAR II station, in Finland promoted the NPF process over the forest environment, which further concluded that a small change in precursor gas emission (either natural or anthropogenic) may lead to the significant impact on cloud and radiative properties.

5. Conclusions

Here, we comprehensively characterized the atmospheric new particle formation at the HACPL site in Mahabaleshwar to provide new insights into the frequency of occurrence of NPF events, the formation and growth rates of charged and neutral clusters and particles, the role of ions in particle formation, and meteorological influence on NPF events.

At HACPL in Mahabaleshwar, the frequency of occurrence of NPF events was the highest in MAM months (22.9%) and the lowest in DJF months (16.9%), which is analogous to previous studies in India and globally except in a few locations wherein NPF event frequently occurred in DJF months. On average, about 20% of days were categorized as undefined event days showing irregularities in particle number size distributions possibly associated with the abrupt mixing of different air masses or the rapid change in meteorological conditions. We then quantified the strength of the observed NPF event days by calculating the formation and growth rates of clusters and particles. The median growth rates of particles in the size range of 3–7 nm, 7–25 nm, and 5–25 nm when averaged over all seasons were 2.9, 4.6, and 4.5 nm h^{-1}, respectively. The size-segregated growth rates of particles were the higher during MAM months as compared with ON and DJF months, replicating the observed seasonal variation in the NPF event frequency. While the particle formation rates of sub-3nm neutral clusters and higher sizes of neutral particles have been widely reported in India, the particle formation rates of 3 nm charged clusters are reported here for the first time in India. The formation rates of positive and negative charged clusters ($\mathbf{J_3^+}$ and $\mathbf{J_3^-}$) at HACPL varied from 3.1 to 294.4 cm^{-3} s^{-1}. The formation rate of 3 nm neutral clusters varied within the same

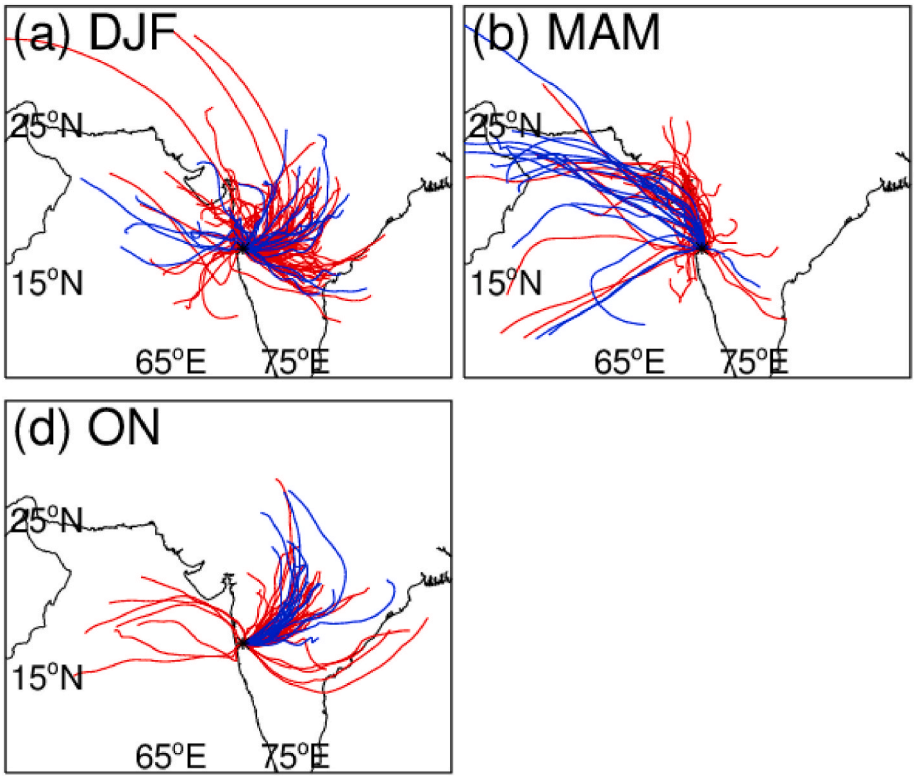

Fig. 8. Three-day air mass backward trajectories starting at 500 m above ground at 6 UTC at the HAPCL site during (a) winter, (b) pre-monsoon, and (d) post-monsoon for NPF events (blue) and non-events events (red) respectively. The measurement site HACPL, Mahabaleshwar is shown by the asterisk sign (*).

order of magnitude between different seasons We further report, for the first time in India, the contribution of ions to particle formation and found that ions play an insignificant role in particle formation at our site analogous to that observed at other sites globally. Further, the general absence of a good positive correlation between the particle growth rates and the particle formation rates, as opposed to most sites globally, indicates the different vapor sources involved in particle formation and growth. This further underlines the existing strong spatiotemporal variability in aerosol and its precursor sources in India. At HACPL in Mahabaleshwar, NPF events generally occurred at higher temperatures and lower relative humidity in all seasons, but the interplay between gas-phase chemistry and atmospheric conditions decides when the NPF event will trigger in the atmosphere. This is corroborated by air mass backward trajectory calculations showing that air mass origin was typically the same between NPF events and non-event days.

CRediT authorship contribution statement

Jeni N. Victor: Conceptualization, Formal analysis, Visualization, Writing – original draft, Writing – review & editing. **Pallavi Buchunde:** Data curation, Formal analysis, Software, Writing – original draft. **Mathew Sebastian:** Data curation, Formal analysis, Software. **Vijay P. Kanawade:** Conceptualization, Methodology, Visualization, Writing – original draft. **Devendraa Siingh:** Conceptualization, Project administration, Writing – review & editing, Supervision. **Subrata Mukherjee:** Data curation, Formal analysis, Software. **Swapnil S. Potdar:** Data curation, Formal analysis, Software. **T. Dharmaraj:** Formal analysis, Funding acquisition, Resources. **Govindan Pandithurai:** Conceptualization, Project administration, Writing – review & editing, Supervision.

Declaration of competing interest

The authors declare that they have no known competing financial interests or personal relationships that could have appeared to influence the work reported in this paper.

Data availability

Data will be made available on request.

Acknowledgments

Indian Institute of Tropical Meteorology, Pune is funded by the Ministry of Earth Sciences, Government of India. The authors are thankful to HACPL, the Mahabaleshwar team for the technical support towards measurements. Authors acknowledge the use of the National Oceanic and Atmospheric Administration (NOAA) Hybrid Single Particle Lagrangian Integrated Trajectory (HYSPLIT) model. VPK and MS acknowledge the Institute of Eminence-University of Hyderabad (sanction no. UoH/IoE/RC1/RC1-20-014). Authors are thankful to Dr. A. K. Kamra for his support and guidance for the installation of NAIS at HACPL, Mahabaleshwar. Authors are thankful to learned referees for their remarks and suggestions.

Appendix A. Supplementary data

Supplementary data to this article can be found online at https://doi.org/10.1016/j.atmosenv.2024.120414.

References

Aslam, M.Y., Mukherjee, S., Kumar, V.A., Patil, R.D., Patil, S.S., Dudhambe, S.D., Saha, S. K., Pandithurai, G., 2021. Seasonal characteristics of boundary layer over a high-altitude rural site in Western India: implications on dispersal of particulate matter. Environ. Sci. Pollut. Res. 28, 35266–35277. https://doi.org/10.1007/s11356-021-13163-7.

Asmi, E., Kivekäs, N., Kerminen, V.M., Komppula, M., Hyvärinen, A.P., Hatakka, J., Viisanen, Y., Lihavainen, H., 2011. Secondary new particle formation in Northern Finland Pallas site between the years 2000 and 2010. Atmos. Chem. Phys. 11, 12959–12972. https://doi.org/10.5194/acp-11-12959-2011.

Baalbaki, R., Pikridas, M., Jokinen, T., Laurila, T., Dada, L., Bezantakos, S., Ahonen, L., Neitola, K., Maisser, A., Bimenyimana, E., Christodoulou, A., Unga, F., Savvides, C., Lehtipalo, K., Kangasluoma, J., Biskos, G., Petäjä, T., Kerminen, V.M., Sciare, J., Kulmala, M., 2021. Towards understanding the characteristics of new particle formation in the Eastern Mediterranean. Atmos. Chem. Phys. 21, 9223–9251. https://doi.org/10.5194/acp-21-9223-2021.

Bianchi, F., Tröstl, J., Junninen, H., Frege, C., Henne, S., Hoyle, C.R., Molteni, U., Herrmann, E., Adamov, A., Bukowiecki, N., Chen, X., Duplissy, J., Gysel, M., Hutterli, M., Kangasluoma, J., Kontkanen, J., Kürten, A., Manninen, H.E., Münch, S., Peräkylä, O., Petäjä, T., Rondo, L., Williamson, C., Weingartner, E., Curtius, J., Worsnop, D.R., Kulmala, M., Dommen, J., Baltensperger, U., 2016. New particle formation in the free troposphere: a question of chemistry and timing. Science 352, 1109–1112. https://doi.org/10.1126/science.aad5456.

Birmili, W., Berresheim, H., Plass-Dülmer, C., Elste, T., Gilge, S., Wiedensohler, A., Uhrner, U., 2003. The Hohenpeissenberg aerosol formation experiment (HAFEX): a long-term study including size-resolved aerosol, H2SO4, OH, and monoterpenes measurements. Atmos. Chem. Phys. 3, 361–376. https://doi.org/10.5194/acp-3-361-2003.

Boy, M., Kulmala, M., 2002. Nucleation events in the continental boundary layer: influence of physical and meteorological parameters. Atmos. Chem. Phys. 2, 1–16. https://doi.org/10.5194/acp-2-1-2002.

Buchunde, P., Safai, P.D., Mukherjee, S., Leena, P.P., Siingh, D., Meena, G.S., Pandithurai, G., 2019. Characterisation of particulate matter at a high-altitude site in southwest India: impact of dust episodes. J. Earth Syst. Sci. 128 https://doi.org/10.1007/s12040-019-1265-8.

Buenrostro Mazon, S., Riipinen, I., Schultz, D.M., Valtanen, M., Maso, M.D., Sogacheva, L., Junninen, H., Nieminen, T., Kerminen, V.M., Kulmala, M., 2009. Classifying previously undefined days from eleven years of aerosol-particle-size distribution data from the SMEAR II station, Hyytiälä, Finland. Atmos. Chem. Phys. 9, 667–676. https://doi.org/10.5194/acp-9-667-2009.

Cai, M.F., Liang, B.L., Sun, Q.B., Zhou, S.Z., Yuan, B., Shao, M., et al., 2021. Contribution of new particle formation to cloud condensation nuclei activity and its controlling factors in a mountain region of inland China. J. Geophys. Res. Atmos. 126, e2020JD034302 https://doi.org/10.1029/2020JD034302.

Chu, B., Matti Kerminen, V., Bianchi, F., Yan, C., Petäjä, T., Kulmala, M., 2019. Atmospheric new particle formation in China. Atmos. Chem. Phys. 19, 115–138. https://doi.org/10.5194/acp-19-115-2019.

Casquero-Vera, J.A., Lyamani, H., Dada, L., Hakala, S., Paasonen, P., Román, R., Fraile, R., Petäjä, T., Olmo-Reyes, F.J., Alados-Arboledas, L., 2020. New particle formation at urban and high-altitude remote sites in the south-eastern Iberian Peninsula. Atmos. Chem. Phys. 20, 14253–14271. https://doi.org/10.5194/acp-20-14253-2020.

Dada, L., Chellapermal, R., Buenrostro Mazon, S., Paasonen, P., Lampilahti, J., E Manninen, H., Junninen, H., Petäjä, T., Kerminen, V.M., Kulmala, M., 2018. Refined classification and characterization of atmospheric new-particle formation events using air ions. Atmos. Chem. Phys. 18, 17883–17893. https://doi.org/10.5194/acp-18-17883-2018.

Dal Maso, M., Kulmala, M., Riipinen, I., Wagner, R., Hussein, T., Aalto, P.P., Lehtinen, K. E.J., 2005. Formation and growth of fresh atmospheric aerosols: eight years of aerosol size distribution data from SMEAR II, Hyytiälä, Finland. Boreal Environ. Res. 10, 323–336.

Deng, C., Fu, Y., Dada, L., Yan, C., Cai, R., Yang, D., Zhou, Y., Yin, R., Lu, Y., Li, X., Qiao, X., Fan, X., Nie, W., Kontkanen, J., Kangasluoma, J., Chu, B., Ding, A., Kerminen, V.M., Paasonen, P., Worsnop, D.R., Bianchi, F., Liu, Y., Zheng, J., Wang, L., Kulmala, M., Jiang, J., 2020. Seasonal characteristics of new particle formation and growth in urban Beijing. Environ. Sci. Technol. 54, 8547–8557. https://doi.org/10.1021/acs.est.0c00808.

Donahue, N.M., Ortega, I.K., Chuang, W., Riipinen, I., Riccobono, F., Schobesberger, S., Dommen, J., Baltensperger, U., Kulmala, M., Worsnop, D.R., Vehkamaki, H., 2013. How do organic vapors contribute to new-particle formation? Faraday Discuss 165, 91–104. https://doi.org/10.1039/c3fd00046j.

Draxler, R.R., Rolph, G.D., 2014. HYSPLIT (HYbrid Single-Particle Lagrangian Integrated Trajectory) Model Access via NOAA ARL READY Website. NOAA Air Resources Laboratory, College Park, MD. http://www.arl.noaa.gov/HYSPLIT.php. NOAA Air Resour. Lab. 8, 26.

Ehn, M., Thornton, J.A., Kleist, E., Sipilä, M., Junninen, H., Pullinen, I., Springer, M., Rubach, F., Tillmann, R., Lee, B., Lopez-Hilfiker, F., Andres, S., Acir, I.H., Rissanen, M., Jokinen, T., Schobesberger, S., Kangasluoma, J., Kontkanen, J., Nieminen, T., Kurtén, T., Nielsen, L.B., Jørgensen, S., Kjaergaard, H.G., Canagaratna, M., Maso, M.D., Berndt, T., Petäjä, T., Wahner, A., Kerminen, V.M., Kulmala, M., Worsnop, D.R., Wildt, J., Mentel, T.F., 2014. A large source of low-volatility secondary organic aerosol. Nature 506, 476–479. https://doi.org/10.1038/nature13032.

Foucart, B., Sellegri, K., Tulet, P., Rose, C., Metzger, J.M., Picard, D., 2018. High occurrence of new particle formation events at the Maïdo high-altitude observatory (2150 m), Réunion (Indian Ocean). Atmos. Chem. Phys. 18, 9243–9261. https://doi.org/10.5194/acp-18-9243-2018.

Gordon, H., Kirkby, J., Baltensperger, U., Bianchi, F., Breitenlechner, M., Curtius, J., Dias, A., Dommen, J., Donahue, N.M., Dunne, E.M., Duplissy, J., Ehrhart, S., Flagan, R.C., Frege, C., Fuchs, C., Hansel, A., Hoyle, C.R., Kulmala, M., Kürten, A., Lehtipalo, K., Makhmutov, V., Molteni, U., Rissanen, M.P., Stozkhov, Y., Tröstl, J., Tsagkogeorgas, G., Wagner, R., Williamson, C., Wimmer, D., Winkler, P.M., Yan, C.,

Carslaw, K.S., 2017. Causes and importance of new particle formation in the present-day and preindustrial atmospheres. J. Geophys. Res. Atmos. 122, 8739–8760. https://doi.org/10.1002/2017JD026844.

Gautam, A.S., Siingh, D., Kamra, A.K., 2017. Statistical analysis of the atmospheric ion concentrations and mobility distributions at a tropical station. Pune. Q. J. Royal Met. Soc. 143, 2116–2128.

Guo, S., Hu, M., Zamora, M.L., Peng, J., Shang, D., Zheng, J., Du, Z., Wu, Z., Shao, M., Zeng, L., Molina, M.J., Zhang, R., 2014. Elucidating severe urban haze formation in China. Proc. Natl. Acad. Sci. U.S.A. 111, 17373–17378. https://doi.org/10.1073/pnas.1419604111.

Hakala, S., Vakkari, V., Bianchi, F., Dada, L., Deng, C., Dällenbach, K.R., Fu, Y., Jiang, J., Kangasluoma, J., Kujansuu, J., Liu, Y., Petäjä, T., Wang, L., Yan, C., Kulmala, M., Paasonen, P., 2022. Observed coupling between air mass history, secondary growth of nucleation mode particles and aerosol pollution levels in Beijing. Environ. Sci. Atmos. 2, 146–164. https://doi.org/10.1039/d1ea00089f.

Hamed, A., Joutsensaari, J., Mikkonen, S., Sogacheva, L., Dal Maso, M., Kulmala, M., Cavalli, F., Fuzzi, S., Facchini, M.C., Decesari, S., Mircea, M., Lehtinen, K.E.J., Laaksonen, A., 2007. Nucleation and growth of new particles in Po Valley, Italy. Atmos. Chem. Phys. 7, 355–376. https://doi.org/10.5194/acp-7-355-2007.

Hirsikko, A., Bergman, T., Laakso, L., Dal Maso, M., Riipinen, I., Hõrrak, U., Kulmala, M., 2007. Identification and classification of the formation of intermediate ions measured in boreal forest. Atmos. Chem. Phys. 7, 201–210. https://doi.org/10.5194/acp-7-201-2007.

Hoppel, W.A., 1985. Ion-aerosol attachment coefficients, ion depletion, and charge distribution on aerosols. J. Geophys. Res. 90, 5917–5923. https://doi.org/10.1029/JD090iD04p05917.

Hõrrak, U., Salm, J., Tammet, H., 2000. Statistical characterization of air ion mobility spectra at Tahkuse Observatory: classification of air ions. J. Geophys. Res. 105, 9291–9302. https://doi.org/10.1029/1999JD901197.

Hõrrak, U., Salm, J., Tammet, H., 2003. Diurnal variation in the concentration of air ions of different mobility classes in a rural area. J. Geophys. Res. 108 https://doi.org/10.1029/2002jd003240.

Israel, H., 1971. Israel program for scientific translations. In: Atmospheric Electricity, pp. 66–73.

Iida, K., Stolzenburg, M.R., McMurry, P.H., Smith, J.N., 2008. Estimating nanoparticle growth rates from size-dependent charged fractions: analysis of new particle formation events in Mexico City. J. Geophys. Res. Atmos. 113 https://doi.org/10.1029/2007JD009260.

Kamra, A.K., Siingh, D., Gautam, A.S., Kanawade, V.P., Tripathi, S.N., Srivastava, A.K., 2015. Atmospheric ions and new particle formation events at a tropical location, Pune, India. Q. J. R. Meteorol. Soc. 141, 3140–3156. https://doi.org/10.1002/qj.2598.

Kamra, A.K., Victor, J.N., Siingh, D., Singh, A., Dharmaraj, T., 2022. Changes in the new particle formation and shrinkage events of the atmospheric ions during the COVID-19 lockdown. Urban Clim. 44.

Kanawade, V.P., Benson, D.R., Lee, S.H., 2012. Statistical analysis of 4-year observations of aerosol sizes in a semi-rural continental environment. Atmos. Environ. 59, 30–38. https://doi.org/10.1016/j.atmosenv.2012.05.047.

Kanawade, V.P., Shika, S., Pöhlker, C., Rose, D., Suman, M.N.S., Gadhavi, H., Kumar, A., Nagendra, S.M.S., Ravikrishna, R., Yu, H., Sahu, L.K., Jayaraman, A., Andreae, M.O., Pöschl, U., Gunthe, S.S., 2014a. Infrequent occurrence of new particle formation at a semi-rural location, Gadanki, in tropical Southern India. Atmos. Environ. 94, 264–273. https://doi.org/10.1016/j.atmosenv.2014.05.046.

Kanawade, V.P., Tripathi, S.N., Siingh, D., Gautam, A.S., Srivastava, A.K., Kamra, A.K., Soni, V.K., Sethi, V., 2014b. Observations of new particle formation at two distinct Indian subcontinental urban locations. Atmos. Environ. 96, 370–379. https://doi.org/10.1016/j.atmosenv.2014.08.001.

Kanawade, V.P., Sebastian, M., Dasari, P., 2022a. Reduction in anthropogenic emissions suppressed new particle formation and growth: insights from the COVID-19 lockdown. J. Geophys. Res. Atmos. 127 https://doi.org/10.1029/2021JD035392.

Kanawade, V.P., Sebastian, M., Hooda, R.K., Hyvärinen, A.P., 2022b. Atmospheric new particle formation in India: current understanding and knowledge gaps. Atmos. Environ. https://doi.org/10.1016/j.atmosenv.2021.118894.

Kerminen, V.M., Paramonov, M., Anttila, T., Riipinen, I., Fountoukis, C., Korhonen, H., Asmi, E., Laakso, L., Lihavainen, H., Swietlicki, E., Svenningsson, B., Asmi, A., Pandis, S.N., Kulmala, M., Petäjä, T., 2012. Cloud condensation nuclei production associated with atmospheric nucleation: a synthesis based on existing literature and new results. Atmos. Chem. Phys. 12, 12037–12059. https://doi.org/10.5194/acp-12-12037-2012.

Kerminen, V.M., Chen, X., Vakkari, V., Petäjä, T., Kulmala, M., Bianchi, F., 2018. Atmospheric new particle formation and growth: review of field observations. Environ. Res. Lett. https://doi.org/10.1088/1748-9326/aadf3c.

Kuang, C., McMurry, P.H., McCormick, A.V., Eisele, F.L., 2008. Dependence of nucleation rates on sulfuric acid vapor concentration in diverse atmospheric locations. J. Geophys. Res. Atmos. 113 https://doi.org/10.1029/2007JD009253.

Kulmala, M., Korhonen, P., Napari, I., Karlsson, A., Berresheim, H., O'Dowd, C.D., 2002. Aerosol formation during PARFORCE: ternary nucleation of H 2so4, NH3, and H2O. J. Geophys. Res. Atmos. 107 https://doi.org/10.1029/2001JD000900.

Kulmala, M., Vehkamäki, H., Petäjä, T., Dal Maso, M., Lauri, A., Kerminen, V.M., Birmili, W., McMurry, P.H., 2004. Formation and growth rates of ultrafine atmospheric particles: a review of observations. J. Aerosol Sci. 35, 143–176. https://doi.org/10.1016/j.jaerosci.2003.10.003.

Kulmala, M., Riipinen, I., Sipilä, M., Manninen, H.E., Petäjä, T., Junninen, H., Dal Maso, M., Mordas, G., Mirme, A., Vana, M., Hirsikko, A., Laakso, L., Harrison, R.M., Hanson, I., Leung, C., Lehtinen, K.E.J., Kerminen, V.M., 2007. Toward direct measurement of atmospheric nucleation. Science 318, 89–92. https://doi.org/10.1126/science.1144124.

Kulmala, M., Petäjä, T., Nieminen, T., Sipilä, M., Manninen, H.E., Lehtipalo, K., Dal Maso, M., Aalto, P.P., Junninen, H., Paasonen, P., Riipinen, I., Lehtinen, K.E.J., Laaksonen, A., Kerminen, V.M., 2012. Measurement of the nucleation of atmospheric aerosol particles. Nat. Protoc. 7, 1651–1667. https://doi.org/10.1038/nprot.2012.091.

Kulmala, M., Kontkanen, J., Junninen, H., Lehtipalo, K., Manninen, H.E., Nieminen, T., Petäjä, T., Sipilä, M., Schobesberger, S., Rantala, P., Franchin, A., Jokinen, T., Järvinen, E., Äijälä, M., Kangasluoma, J., Hakala, J., Aalto, P.P., Paasonen, P., Mikkilä, J., Vanhanen, J., Aalto, J., Hakola, H., Makkonen, U., Ruuskanen, T., Mauldin, R.L., Duplissy, J., Vehkamäki, H., Bäck, J., Kortelainen, A., Riipinen, I., Kurtén, T., Johnston, M.V., Smith, J.N., Ehn, M., Mentel, T.F., Lehtinen, K.E.J., Laaksonen, A., Kerminen, V.M., Worsnop, D.R., 2013. Direct observations of atmospheric aerosol nucleation. Science 339, 943–946. https://doi.org/10.1126/science.1227385.

Kulmala, M., Petäjä, T., Ehn, M., Thornton, J., Sipilä, M., Worsnop, D.R., Kerminen, V.M., 2014. Chemistry of atmospheric nucleation: on the recent advances on precursor characterization and atmospheric cluster composition in connection with atmospheric new particle formation. Annu. Rev. Phys. Chem. 65, 21–37. https://doi.org/10.1146/annurev-physchem-040412-110014.

Kulmala, M., 2015. Atmospheric chemistry: China's choking cocktail. Nature. https://doi.org/10.1038/526497a.

Kulmala, M., Dada, L., Daellenbach, K.R., Yan, C., Stolzenburg, D., Kontkanen, J., Ezhova, E., Hakala, S., Tuovinen, S., Kokkonen, T.V., Kurppa, M., Cai, R., Zhou, Y., Yin, R., Baalbaki, R., Chan, T., Chu, B., Deng, C., Fu, Y., Ge, M., He, H., Heikkinen, L., Junninen, H., Liu, Y., Lu, Y., Nie, W., Rusanen, A., Vakkari, V., Wang, Y., Yang, G., Yao, L., Zheng, J., Kujansuu, J., Kangasluoma, J., Petaja, T., Paasonen, P., Jarvi, L., Worsnop, D., Ding, A., Liu, Y., Wang, L., Jiang, J., Bianchi, F., Kerminen, V.M., 2021. Is reducing new particle formation a plausible solution to mitigate particulate air pollution in Beijing and other Chinese megacities? Faraday Discuss 226, 334–347. https://doi.org/10.1039/d0fd00078g.

Kulmala, M., Junninen, H., Dada, L., Salma, I., Weidinger, T., Thén, W., Vörösmarty, M., Komsaare, K., Stolzenburg, D., Cai, R., Yan, C., Li, X., Deng, C., Jiang, J., Petäjä, T., Nieminen, T., Kerminen, V.M., 2022a. Quiet new particle formation in the atmosphere. Front. Environ. Sci. 10 https://doi.org/10.3389/fenvs.2022.912385.

Kulmala, M., Stolzenburg, D., Dada, L., Cai, R., Kontkanen, J., Yan, C., Kangasluoma, J., Ahonen, L.R., Gonzalez-Carracedo, L., Sulo, J., Tuovinen, S., Deng, C., Li, Y., Lehtipalo, K., Lehtinen, K.E.J., Petäjä, T., Winkler, P.M., Jiang, J., Kerminen, V.M., 2022b. Towards a concentration closure of sub-6 nm aerosol particles and sub-3 nm atmospheric clusters. J. Aerosol Sci. 159 https://doi.org/10.1016/j.jaerosci.2021.105878.

Kürten, A., Bianchi, F., Almeida, J., Kupiainen-Määttä, O., Dunne, E.M., Duplissy, J., Williamson, C., Barmet, P., Breitenlechner, M., Dommen, J., Donahue, N.M., Flagan, R.C., Franchin, A., Gordon, H., Hakala, J., Hansel, A., Heinritzi, M., Ickes, L., Jokinen, T., Kangasluoma, J., Kim, J., Kirkby, J., Kupc, A., Lehtipalo, K., Leiminger, M., Makhmutov, V., Onnela, A., Ortega, I.K., Petäjä, T., Praplan, A.P., Riccobono, F., Rissanen, M.P., Rondo, L., Schnitzhofer, R., Schobesberger, S., Smith, J.N., Steiner, G., Stozhkov, Y., Tomé, A., Tröstl, J., Tsagkogeorgas, G., Wagner, P.E., Wimmer, D., Ye, P., Baltensperger, U., Carslaw, K., Kulmala, M., Curtius, J., 2016. Experimental particle formation rates spanning tropospheric sulfuric acid and ammonia abundances, ion production rates, and temperatures. J. Geophys. Res. 121 (12) https://doi.org/10.1002/2015JD023908, 377-12,400.

Laakso, L., Laakso, H., Aalto, P.P., Keronen, P., Petëjä, T., Nieminen, T., Pohja, T., Siivola, E., Kulmala, M., Kgabi, N., Molefe, M., Mabaso, D., Phalatse, D., Pienaar, K., Kerminen, V.M., 2008. Basic characteristics of atmospheric particles, trace gases and meteorology in a relatively clean Southern African Savannah environment. Atmos. Chem. Phys. 8, 4823–4839. https://doi.org/10.5194/acp-8-4823-2008.

Leena, P.P., Anil Kumar, V., Dani, K.K., Sombawne, S.M., Murugavel, P., Pandithurai, G., 2017. Evidence of new particle formation during post monsoon season over a high-altitude site of the Western Ghats, India. Toxicol. Environ. Chem. 99, 652–664. https://doi.org/10.1080/02772248.2016.1274031.

Lehtipalo, K., Yan, C., Dada, L., Bianchi, F., Xiao, M., Wagner, R., Stolzenburg, D., Ahonen, L.R., Amorim, A., Baccarini, A., Bauer, P.S., Baumgartner, B., Bergen, A., Bernhammer, A.K., Breitenlechner, M., Brilke, S., Buchholz, A., Mazon, S.B., Chen, D., Chen, X., Dias, A., Dommen, J., Draper, D.C., Duplissy, J., Ehn, M., Finkenzeller, H., Fischer, L., Frege, C., Fuchs, C., Garmash, O., Gordon, H., Hakala, J., He, X., Heikkinen, L., Heinritzi, M., Helm, J.C., Hofbauer, V., Hoyle, C.R., Jokinen, T., Kangasluoma, J., Kerminen, V.M., Kim, C., Kirkby, J., Kontkanen, J., Kürten, A., Lawler, M.J., Mai, H., Mathot, S., Mauldin, R.L., Molteni, U., Nichman, L., Nie, W., Nieminen, T., Ojdanic, A., Onnela, A., Passananti, M., Petäjä, T., Piel, F., Pospisilova, V., Quéléver, L.L.J., Rissanen, M.P., Rose, C., Sarnela, N., Schallhart, S., Schuchmann, S., Sengupta, K., Simon, M., Sipilä, M., Tauber, C., Tomé, A., Tröstl, J., Väisänen, O., Vogel, A.L., Volkamer, R., Wagner, A.C., Wang, M., Weitz, L., Wimmer, D., Ye, P., Ylisirniö, A., Zha, Q., Carslaw, K.S., Curtius, J., Donahue, N.M., Flagan, R.C., Hansel, A., Riipinen, I., Virtanen, A., Winkler, P.M., Baltensperger, U., Kulmala, M., Worsnop, D.R., 2018. Multicomponent new particle formation from sulfuric acid, ammonia, and biogenic vapors. Sci. Adv. 4 https://doi.org/10.1126/sciadv.aau5363.

Lv, G., Sui, X., Chen, J., Jayaratne, R., Mellouki, A., 2018. Investigation of new particle formation at the summit of Mt. Tai, China. Atmos. Chem. Phys. 18, 2243–2258. https://doi.org/10.5194/acp-18-2243-2018.

Manninen, H.E., Nieminen, T., Riipinen, I., Yli-Juuti, T., Gagné, S., Asmi, E., Aalto, P.P., Petäjä, T., Kerminen, V.M., Kulmala, M., 2009. Charged and total particle formation and growth rates during EUCAARI 2007 campaign in Hyytiälä. Atmos. Chem. Phys. 9, 4077–4089. https://doi.org/10.5194/acp-9-4077-2009.

Manninen, H.E., Nieminen, T., Asmi, E., Gagné, S., Häkkinen, S., Lehtipalo, K., Aalto, P., Vana, M., Mirme, A., Mirme, S., Hõrrak, U., Plass-Dülmer, C., Stange, G., Kiss, G., Hoffer, A., Töro, N., Moerman, M., Henzing, B., De Leeuw, G., Brinkenberg, M., Kouvarakis, G.N., Bougiatioti, A., Mihalopoulos, N., O'Dowd, C., Ceburnis, D., Arneth, A., Svenningsson, B., Swietlicki, E., Tarozzi, L., Decesari, S., Facchini, M.C., Birmili, W., Sonntag, A., Wiedensohler, A., Boulon, J., Sellegri, K., Laj, P., Gysel, M., Bukowiecki, N., Weingartner, E., Wehrle, G., Laaksonen, A., Hamed, A., Joutsensaari, J., Petäjä, T., Kerminen, V.M., Kulmala, M., 2010. EUCAARI ion spectrometer measurements at 12 European sites-analysis of new particle formation events. Atmos. Chem. Phys. 10, 7907–7927. https://doi.org/10.5194/acp-10-7907-2010.

Mirme, A., Tamm, E., Mordas, G., Vana, M., Uin, J., Mirme, S., Bernotas, T., Laakso, L., Hirsikko, A., Kulmala, M., 2007. A wide-range multi-channel air ion spectrometer. Boreal Environ. Res. 12, 247–264.

Mirme, S., Mirme, A., 2013. The mathematical principles and design of the NAIS - a spectrometer for the measurement of cluster ion and nanometer aerosol size distributions. Atmos. Meas. Tech. 6, 1061–1071. https://doi.org/10.5194/amt-6-1061-2013.

Mukherjee, S., Singla, V., Pandithurai, G., Safai, P.D., Meena, G.S., Dani, K.K., Anil Kumar, V., 2018. Seasonal variability in chemical composition and source apportionment of sub-micron aerosol over a high altitude site in Western Ghats, India. Atmos. Environ. 180, 79–92. https://doi.org/10.1016/j.atmosenv.2018.02.048.

Mukherjee, S., Singla, V., Meena, G.S., Aslam, M.Y., Safai, P.D., Buchunde, P., Vasudevan, A.K., Jena, C.K., Ghude, S.D., Dani, K., Pandithurai, G., 2020. Sub micron aerosol variability and its ageing process at a high altitude site in India: impact of meteorological conditions. Environ. Pollut. 265 https://doi.org/10.1016/j.envpol.2020.115019.

Nieminen, T., Asmi, A., Aalto, P.P., Keronen, P., Petäjä, T., Kulmala, M., Kerminen, V.M., Nieminen, T., Dal Maso, M., 2014. Trends in atmospheric new-particle formation: 16 years of observations in a boreal-forest environment. Boreal Environ. Res. 19, 191–214.

Nepolian, J.V., Siingh, D., Singh, R.P., Gautam, A.S., Gautam, S., 2021. Analysis of positive and negative atmospheric air ions during New Particle Formation (NPF) events over Urban City of India. Aerosol Sci. Eng. 5, 460–477. https://doi.org/10.1007/s41810-021-00115-4.

Paasonen, P., Nieminen, T., Asmi, E., Manninen, H.E., Petäjä, T., Plass-Dülmer, C., Flentje, H., Birmili, W., Wiedensohler, A., Hõrrak, U., Metzger, A., Hamed, A., Laaksonen, A., Facchini, M.C., Kerminen, V.M., Kulmala, M., 2010. On the roles of sulphuric acid and low-volatility organic vapours in the initial steps of atmospheric new particle formation. Atmos. Chem. Phys. 10, 11223–11242. https://doi.org/10.5194/acp-10-11223-2010.

Petäjä, T., Tabakova, K., Manninen, A., Ezhova, E., O'Connor, E., Moisseev, D., Sinclair, V.A., Backman, J., Levula, J., Luoma, K., Virkkula, A., Paramonov, M., Räty, M., Äijälä, M., Heikkinen, L., Ehn, M., Sipilä, M., Yli-Juuti, T., Virtanen, A., Ritsche, M., Hickmon, N., Pulik, G., Rosenfeld, D., Worsnop, D.R., Bäck, J., Kulmala, M., Kerminen, V.M., 2022. Influence of biogenic emissions from boreal forests on aerosol–cloud interactions. Nat. Geosci. 15, 42–47. https://doi.org/10.1038/s41561-021-00876-0.

Pierce, J.R., Adams, P.J., 2007. Efficiency of cloud condensation nuclei formation from ultrafine particles. Atmos. Chem. Phys. 7, 1367–1379. https://doi.org/10.5194/acp-7-1367-2007.

Roldin, P., Ehn, M., Kurtén, T., Olenius, T., Rissanen, M.P., Sarnela, N., Elm, J., Rantala, P., Hao, L., Hyttinen, N., Heikkinen, L., Worsnop, D.R., Pichelstorfer, L., Xavier, C., Clusius, P., Öström, E., Petäjä, T., Kulmala, M., Vehkamäki, H., Virtanen, A., Riipinen, I., Boy, M., 2019. The role of highly oxygenated organic molecules in the Boreal aerosol-cloud-climate system. Nat. Commun. 10 https://doi.org/10.1038/s41467-019-12338-8.

Rose, C., Sellegri, K., Velarde, F., Moreno, I., Ramonet, M., Weinhold, K., Krejci, R., Andrade, M., Wiedensohler, A., Laj, P., 2015. Frequent nucleation events at the high altitude station of Chacaltaya (5240m a.s.l.), Bolivia. Atmos. Environ. 102, 18–29. https://doi.org/10.1016/j.atmosenv.2014.11.015.

Rose, C., Zha, Q., Dada, L., Yan, C., Lehtipalo, K., Junninen, H., Mazon, S.B., Jokinen, T., Sarnela, N., Sipilä, M., Petäjä, T., Kerminen, V.M., Bianchi, F., Kulmala, M., 2018. Observations of biogenic ion-induced cluster formation in the atmosphere. Sci. Adv. 4 https://doi.org/10.1126/sciadv.aar5218.

Schobesberger, S., Junninen, H., Bianchi, F., Lönn, G., Ehn, M., Lehtipalo, K., Dommen, J., Ehrhart, S., Ortega, I.K., Franchin, A., Nieminen, T., Riccobono, F., Hutterli, M., Duplissy, J., Almeida, J., Amorim, A., Breitenlechner, M., Downard, A. J., Dunne, E.M., Flagan, R.C., Kajos, M., Keskinen, H., Kirkby, J., Kupc, A., Kürten, A., Kurtén, T., Laaksonen, A., Mathot, S., Onnela, A., Praplan, A.P., Rondo, L., Santos, F.D., Schallhart, S., Schnitzhofer, R., Sipilä, M., Tomé, A., Tsagkogeorgas, G., Vehkamäki, H., Wimmer, D., Baltensperger, U., Carslaw, K.S., Curtius, J., Hansel, A., Petäjä, T., Kulmala, M., Donahue, N.M., Worsnop, D.R., 2013. Molecular understanding of atmospheric particle formation from sulfuric acid and large oxidized organic molecules. Proc. Natl. Acad. Sci. U.S.A. 110, 17223–17228. https://doi.org/10.1073/pnas.1306973110.

Sebastian, M., Kanawade, V.P., Soni, V.K., Asmi, E., Westervelt, D.M., Vakkari, V., Hyvärinen, A.P., Pierce, J.R., Hooda, R.K., 2021a. New particle formation and growth to climate-relevant aerosols at a background remote site in the western himalaya. J. Geophys. Res. Atmos. 126 https://doi.org/10.1029/2020JD033267.

Sebastian, M., Kanawade, V.P., Pierce, J.R., 2021b. Observation of sub-3nm particles and new particle formation at an urban location in India. Atmos. Environ. 256 https://doi.org/10.1016/j.atmosenv.2021.118460.

Sebastian, M., Kompalli, S.K., Kumar, V.A., Jose, S., Babu, S.S., Pandithurai, G., Singh, S., Hooda, R.K., Soni, V.K., Pierce, J.R., Vakkari, V., Asmi, E., Westervelt, D.M., Hyvärinen, A.P., Kanawade, V.P., 2022. Observations of particle number size distributions and new particle formation in six Indian locations. Atmos. Chem. Phys. 22, 4491–4508. https://doi.org/10.5194/acp-22-4491-2022.

Sellegri, K., Rose, C., Marinoni, A., Lupi, A., Wiedensohler, A., Andrade, M., Bonasoni, P., Laj, P., 2019. New particle formation: a review of ground-based observations at mountain research stations. Atmosphere 10, 10.330/atmos10090493.

Shang, D., Hu, M., Zheng, J., Qin, Y., du, Z., Li, M., Fang, J., Peng, J., Wu, Y., Lu, S., Guo, S., 2018. Particle size distribution and new particle formation under influence of biomass burning at a high altitude background site of Mt. Yulong (3410m) in China. Atmos. Chem. Phys. 18, 15687–15703. https://doi.org/10.5194/acp-18-15687-2018.

Shen, X.J., Sun, J.Y., Zhang, Y.M., Wehner, B., Nowak, A., Tuch, T., Zhang, X.C., Wang, T.T., Zhou, H.G., Zhang, X.L., Dong, F., Birmili, W., Wiedensohler, A., 2011. First long-term study of particle number size distributions and new particle formation events of regional aerosol in the North China Plain. Atmos. Chem. Phys. 11, 1565–1580. https://doi.org/10.5194/acp-11-1565-2011.

Singh, A., Raj, S.S., Panda, U., Kommula, S.M., Jose, C., Liu, T., Huang, S., Swain, B., Pöhlker, M.L., Reyes-Villegas, E., Ojha, N., Vaishya, A., Bigi, A., Ravikrishna, R., Zhu, Q., Shi, L., Allen, J., Martin, S.T., McFiggans, G., Andreae, M.O., Pöschl, U., Coe, H., Bianchi, F., Su, H., Kanawade, V.P., Liu, P., Gunthe, S.S., 2023. Rapid growth and high cloud-forming potential of anthropogenic sulfate aerosol in a thermal power plant plume during COVID lockdown in India, npj. Clim. Atmosph. Sci. 6 (2023), 109. https://doi.org/10.1038/s41612-023-00430-2.

Siingh, D., Pant, V., Kamra, A.K., 2011. The ion–aerosol interactions from the ion mobility and aerosol particle size distribution measurements on January 17 and February 18, 2005 at Maitri, Antarctica–A case study. J. Earth Syst. Sci. 120, 735–754.

Siingh, D., Gautam, A.S., Kamra, A.K., Komsaare, K., 2013. Nucleation events for the formation of charged aerosol particles at a tropical station - preliminary results. Atmos. Res. 132–133, 239–252. https://doi.org/10.1016/j.atmosres.2013.05.024.

Siingh, D., Gautam, A.S., Buchunde, P.S., Kamra, A.K., 2018. Classification of the new particle formation events observed at a tropical site, Pune, India. Atmos. Environ. 190, 10–22. https://doi.org/10.1016/j.atmosenv.2018.07.025.

Smith, J.N., Barsantia, K.C., Friedlia, H.R., Ehnd, M., Kulmala, M., Collins, D.R., Scheckman, J.H., Williams, B.J., McMurry, P.H., 2010. Observations of aminium salts in atmospheric nanoparticles and possible climatic implications. Proc. Natl. Acad. Sci. U.S.A. 107, 6634–6639. https://doi.org/10.1073/pnas.0912127107.

Stanier, C.O., Khlystov, A.Y., Pandis, S.N., 2004. Nucleation events during the Pittsburgh Air Quality Study: description and relation to key meteorological, gas phase, and aerosol parameters. Aerosol Sci. Technol. 38, 253–264. https://doi.org/10.1080/02786820390229570.

Sullivan, R.C., Crippa, P., Matsui, H., Leung, L.R., Zhao, C., Thota, A., Pryor, S.C., 2018. New particle formation leads to cloud dimming. npj Clim. Atmos. Sci. 1 https://doi.org/10.1038/s41612-018-0019-7.

Suni, T., Kulmala, M., Hirsikko, A., Bergman, T., Laakso, L., Aalto, P.P., Leuning, R., Cleugh, H., Zegelin, S., Hughes, D., Van Gorsel, E., Kitchen, M., Vana, M., Hörrak, U., Mirme, S., Mirme, A., Sevanto, S., Twining, J., Tadros, C., 2008. Formation and characteristics of ions and charged aerosol particles in a native Australian Eucalypt forest. Atmos. Chem. Phys. 8, 129–139. https://doi.org/10.5194/acp-8-129-2008.

Tammet, H., 1995. Size and mobility of nanometer particles, clusters and ions. J. Aerosol Sci. 26, 459–475. https://doi.org/10.1016/0021-8502(94)00121-E.

Tröstl, J., Herrmann, E., Frege, C., Bianchi, F., Molteni, U., Bukowiecki, N., Hoyle, C.R., Steinbacher, M., Weingartner, E., Dommen, J., Gysel, M., Baltensperger, U., 2016. Contribution of new particle formation to the total aerosol concentration at the high-altitude site Jungfraujoch (3580 m asl, Switzerland). J. Geophys. Res. Atmos. 121, 11692–611711. https://doi.org/10.1002/2015jd024637.

Tunved, P., Hansson, H.C., Kerminen, V.M., Ström, J., Dal Maso, M., Lihavainen, H., Viisanen, Y., Aalto, P.P., Komppula, M., Kulmala, M., 2006. High natural aerosol loading over boreal forests. Science 312 (80), 261–263. https://doi.org/10.1126/science.1123052.

Wagner, R., Manninen, H.E., Franchin, A., Lehtipalo, K., Mirme, S., Steiner, G., Petäjä, T., Kulmala, M., 2016. On the accuracy of ion measurements using a Neutral cluster and Air Ion Spectrometer. Boreal Environ. Res. 21, 230–241.

Wagner, R., Yan, C., Lehtipalo, K., Duplissy, J., Nieminen, T., Kangasluoma, J., Ahonen, L.R., Dada, L., Kontkanen, J., Manninen, H.E., Dias, A., Amorim, A., Bauer, P.S., Bergen, A., Bernhammer, A.K., Bianchi, F., Brilke, S., Buenrostro Mazon, S., Chen, X., Draper, D.C., Fischer, L., Frege, C., Fuchs, C., Garmash, O., Gordon, H., Hakala, J., Heikkinen, L., Heinritzi, M., Hofbauer, V., Hoyle, C.R., Kirkby, J., Kürten, A., Kvashnin, A.N., Laurila, T., Lawler, M.J., Mai, H., Makhmutov, V., Mauldin, R., Molteni, U., Nichman, L., Nie, W., Ojdanic, A., Onnela, A., Piel, F., Quéléver, L.L.J., Rissanen, M.P., Sarnela, N., Schallhart, S., Sengupta, K., Simon, M., Stolzenburg, D., Stozhkov, Y., Tröstl, J., Viisanen, Y., Vogel, A.L., Wagner, A.C., Xiao, M., Ye, P., Baltensperger, U., Curtius, J., Donahue, N.M., Flagan, R.C., Gallagher, M., Hansel, A., Smith, J.N., Tomé, A., Winkler, P.M., Worsnop, D., Ehn, M., Sipilä, M., Kerminen, V.M., Petäjä, T., Kulmala, M., 2017. The role of ions in new particle formation in the CLOUD chamber. Atmos. Chem. Phys. 17, 15181–15197. https://doi.org/10.5194/acp-17-15181-2017.

Wang, Z.B., Hu, M., Sun, J.Y., Wu, Z.J., Yue, D.L., Shen, X.J., Zhang, Y.M., Pei, X.Y., Cheng, Y.F., Wiedensohler, A., 2013. Characteristics of regional new particle formation in urban and regional background environments in the North China Plain. Atmos. Chem. Phys. 13, 12495–12506. https://doi.org/10.5194/acp-13-12495-2013.

Wang, Z., Hu, M., Wu, Z., Yue, D., 2013. Reasearch on the formation mechanisms of new particles in the atmosphere. Acta Chim. Sin. https://doi.org/10.6023/A12121062.

Wang, Z., Wu, Z., Yue, D., Shang, D., Guo, S., Sun, J., Ding, A., Wang, L., Jiang, J., Guo, H., Gao, J., Cheung, H.C., Morawska, L., Keywood, M., Hu, M., 2017. New particle formation in China: current knowledge and further directions. Sci. Total Environ. 577, 258–266. https://doi.org/10.1016/j.scitotenv.2016.10.177.

Xiao, S., Wang, M.Y., Yao, L., Kulmala, M., Zhou, B., Yang, X., Chen, J.M., Wang, D.F., Fu, Q.Y., Worsnop, D.R., Wang, L., 2015. Strong atmospheric new particle formation in winter in urban Shanghai, China. Atmos. Chem. Phys. 15, 1769–1781. https://doi.org/10.5194/acp-15-1769-2015.

Xiao, M., Hoyle, C.R., Dada, L., Stolzenburg, D., Kürten, A., Wang, M., Lamkaddam, H., Garmash, O., Mentler, B., Molteni, U., Baccarini, A., Simon, M., He, X.C., Lehtipalo, K., Ahonen, L.R., Baalbaki, R., Bauer, P.S., Beck, L., Bell, D., Bianchi, F., Brilke, S., Chen, D., Chiu, R., Dias, A., Duplissy, J., Finkenzeller, H., Gordon, H., Hofbauer, V., Kim, C., Koenig, T.K., Lampilahti, J., Lee, C.P., Li, Z., Mai, H., Makhmutov, V., Manninen, H.E., Marten, R., Mathot, S., Mauldin, R.L., Nie, W., Onnela, A., Partoll, E., Petäjä, T., Pfeifer, J., Pospisilova, V., Quéléver, L.L.J., Rissanen, M., Schobesberger, S., Schuchmann, S., Stozhkov, Y., Tauber, C., Tham, Y. J., Tomé, A., Vazquez-Pufleau, M., Wagner, A.C., Wagner, R., Wang, Y., Weitz, L., Wimmer, D., Wu, Y., Yan, C., Ye, P., Ye, Q., Zha, Q., Zhou, X., Amorim, A., Carslaw, K., Curtius, J., Hansel, A., Volkamer, R., Winkler, P.M., Flagan, R.C., Kulmala, M., Worsnop, D.R., Kirkby, J., Donahue, N.M., Baltensperger, U., El Haddad, I., Dommen, J., 2021. The driving factors of new particle formation and growth in the polluted boundary layer. Atmos. Chem. Phys. 21, 14275–14291. https://doi.org/10.5194/acp-21-14275-2021.

Yadav, S.K., Kompalli, S.K., Gurjar, B.R., Mishra, R.K., 2021. Aerosol number concentrations and new particle formation events over a polluted megacity during the COVID-19 lockdown. Atmos. Environ. 259, 118526. https://doi.org/10.1016/j.atmosenv.2021.118526.

Yli-Juuti, T., Riipinen, N., Aalto, P.P., Nieminen, T., Maenhaut, W., Janssens, I.A., Claeys, M., Salma, I., Ocskay, R., Hoffer, A., Lmre, K., Kulmala, M., 2009. Characteristics of new particle formation events and cluster ions at K-puszta, Hungary. Boreal Environ. Res. 14, 683–698.

Yu, H., Zhou, L., Dai, L., Shen, W., Dai, W., Zheng, J., Ma, Y., Chen, M., 2016. Nucleation and growth of sub-3 nm particles in the polluted urban atmosphere of a megacity in China. Atmos. Chem. Phys. 16, 2641–2657. https://doi.org/10.5194/acp-16-2641-2016.

Yue, D.L., Hu, M., Wang, Z.B., Wen, M.T., Guo, S., Zhong, L.J., Wiedensohler, A., Zhang, Y.H., 2013. Comparison of particle number size distributions and new particle formation between the urban and rural sites in the PRD region, China. Atmos. Environ. 76, 181–188. https://doi.org/10.1016/j.atmosenv.2012.11.018.

Zhang, Y., Liu, P., Liu, X.H., Jacobson, M.Z., McMurry, P.H., Yu, F., Yu, S., Schere, K.L., 2010. A comparative study of nucleation parameterizations: 2. Three-dimensional model application and evaluation. J. Geophys. Res. Atmos. 115 https://doi.org/10.1029/2010JD014151.

Zhao, B., Shrivastava, M., Donahue, N.M., Gordon, H., Schervish, M., Shilling, J.E., Zaveri, R.A., Wang, J., Andreae, M.O., Zhao, C., Gaudet, B., Liu, Y., Fan, J., Fast, J.D., 2020. High concentration of ultrafine particles in the Amazon free troposphere produced by organic new particle formation. Proc. Natl. Acad. Sci. U.S.A. 117, 25344–25351. https://doi.org/10.1073/pnas.2006716117.

Zhou, Y., Hakala, S., Yan, C., Gao, Y., Yao, X., Chu, B., Chan, T., Kangasluoma, J., Gani, S., Kontkanen, J., Paasonen, P., Liu, Y., Petäjä, T., Kulmala, M., Dada, L., 2021. Measurement report: new particle formation characteristics at an urban and a mountain station in northern China. Atmos. Chem. Phys. 21, 17885–17906. https://doi.org/10.5194/acp-21-17885-2021.

Zhu, Y., Yan, C., Zhang, R., Wang, Z., Zheng, M., Gao, H., Gao, Y., Yao, X., 2017. Simultaneous measurements of new particle formation at 1s time resolution at a street site and a rooftop site. Atmos. Chem. Phys. 17, 9469–9484. https://doi.org/10.5194/acp-17-9469-2017.